

1

2

3 **Natural depletion of H1 in sex cells causes DNA demethylation, heterochromatin**  
4 **decondensation and transposon activation**

5 **Authors:** Shengbo He, Martin Vickers, Jingyi Zhang, Xiaoqi Feng\*

6 **Affiliation:** Department of Cell and Developmental Biology, John Innes Centre, Norwich  
7 NR4 7UH, UK.

8 \*For correspondence: Xiaoqi Feng ([xiaoqi.feng@jic.ac.uk](mailto:xiaoqi.feng@jic.ac.uk))

9

## 10 **Abstract**

11 Transposable elements (TEs), the movement of which can damage the genome, are  
12 epigenetically silenced in eukaryotes. Intriguingly, TEs are activated in the sperm companion  
13 cell – vegetative cell (VC) – of the flowering plant *Arabidopsis thaliana*. However, the extent  
14 and mechanism of this activation are unknown. Here we show that about 100 heterochromatic  
15 TEs are activated in VCs, mostly by DEMETER-catalyzed DNA demethylation. We further  
16 demonstrate that DEMETER access to some of these TEs is permitted by the natural depletion  
17 of linker histone H1 in VCs. Ectopically expressed H1 suppresses TEs in VCs by reducing  
18 DNA demethylation and via a methylation-independent mechanism. We demonstrate that H1  
19 is required for heterochromatin condensation in plant cells and show that H1 overexpression  
20 creates heterochromatic foci in the VC progenitor cell. Taken together, our results demonstrate  
21 that the natural depletion of H1 during male gametogenesis facilitates DEMETER-directed  
22 DNA demethylation, heterochromatin relaxation, and TE activation.

23

## 24 **Introduction**

25 Large proportions of most eukaryotic genomes are comprised of transposable elements (TEs),  
26 mobile genetic fragments that can jump from one location to another. For example, TEs  
27 comprise approximately 50% of the human genome (Lander et al., 2001; Venter et al., 2001),  
28 and more than 85% of the genomes in crops such as wheat and maize (Schnable et al., 2009;  
29 Wicker et al., 2018). Regarded as selfish and parasitic, activities of TEs compromise genome  
30 stability, disrupt functional genes, and are often associated with severe diseases including  
31 cancers in animals (Anwar, Wulaningsih, & Lehmann, 2017). To safeguard genome integrity,  
32 eukaryotic hosts have evolved efficient epigenetic mechanisms, including DNA methylation,  
33 to suppress TEs (He, Chen, & Zhu, 2011; Law & Jacobsen, 2010). Curiously, recent studies  
34 point to episodes of TE activation that occur in specific cell types and/or particular  
35 developmental stages (Garcia-Perez, Widmann, & Adams, 2016; Martinez & Slotkin, 2012).  
36 These TE activation events provide unique opportunities to understand epigenetic silencing  
37 mechanisms, and the co-evolution between TEs and their hosts.

38 Developmental TE activation has been shown in mammalian embryos, germlines and brain  
39 cells. In pre-implantation embryos and the fetal germline, LINE-1 retrotransposons are highly  
40 expressed despite relatively low levels of transposition (Fadloun et al., 2013; Kano et al., 2009;  
41 Percharde, Wong, & Ramalho-Santos, 2017; Richardson et al., 2017). Recently, LINE-1 RNA  
42 was shown to play a key regulatory role in promoting pre-implantation embryo development  
43 in mice (Percharde et al., 2018). LINE-1 elements have also been shown to transcribe and  
44 mobilise in neuronal precursor cells in mice and human (Coufal et al., 2009; Muotri et al.,  
45 2005). The underlying mechanism of such cell-specific TE activation is still unclear.  
46 Hypomethylation at LINE-1 promoters in neurons has been proposed to contribute (Coufal et  
47 al., 2009), and possibly the availability of transcription factors (Muotri et al., 2005; Richardson,

48 Morell, & Faulkner, 2014). The frequency of LINE-1 retrotransposition in mammalian brain is  
49 still under debate, however, it is conceivable that LINE-1 activities may serve to promote  
50 genetic diversity among cells of a highly complex organ like the brain (Garcia-Perez et al.,  
51 2016; Richardson et al., 2014; Singer, McConnell, Marchetto, Coufal, & Gage, 2010).

52 One of the best demonstrated cases of developmental TE activation occurs in the male  
53 gametophyte of flowering plants, pollen grains. Pollen are products of male gametogenesis,  
54 which initiates from haploid meiotic products called microspores. Each microspore undergoes  
55 an asymmetric mitosis to generate a bicellular pollen comprised of a large vegetative cell (VC)  
56 and a small generative cell engulfed by the VC (Berger & Twell, 2011). Subsequently the  
57 generative cell divides again mitotically to produce two sperm. Upon pollination, the VC  
58 develops into a pollen tube to deliver the sperm to meet the female cells, and subsequently  
59 degenerates. In the mature tricellular pollen of *Arabidopsis thaliana*, several TEs were found  
60 activated and transposed (Slotkin et al., 2009). Enhancer/gene trap insertions into TEs showed  
61 specific reporter activity in the VC, and TE transpositions detected in pollen were absent in  
62 progeny (Slotkin et al., 2009). These results demonstrated TE activation in pollen is confined  
63 to the VC. TE expression in the short-lived VC has been proposed to promote the production  
64 of small RNAs, which may be transported into sperm to reinforce the silencing of cognate TEs  
65 (Calarco et al., 2012; Ibarra et al., 2012; Martinez, Panda, Kohler, & Slotkin, 2016; Slotkin et  
66 al., 2009). However, TE transcription in the VC has not been comprehensively investigated,  
67 hindering our understanding of this phenomenon.

68 The mechanisms underlying TE reactivation in the VC are also unknown. One proposed  
69 mechanism is the absence of the Snf2 family nucleosome remodeler DDM1 (Slotkin et al.,  
70 2009). DDM1 functions to overcome the impediment of nucleosomes and linker histone H1 to  
71 DNA methyltransferases (Lyons & Zilberman, 2017; Zemach et al., 2013). Loss of DDM1

72 leads to DNA hypomethylation and massive TE derepression in somatic tissues (Jeddeloh,  
73 Stokes, & Richards, 1999; Lippman et al., 2004; Tsukahara et al., 2009; Zemach et al., 2013).  
74 However, global DNA methylation in the VC is comparable to that of microspores and  
75 substantially higher than in somatic tissues (Calarco et al., 2012; Hsieh et al., 2016; Ibarra et  
76 al., 2012). This suggests that DDM1 is present during the first pollen mitosis that produces the  
77 VC, so its later absence is unlikely to cause TE activation.

78 A plausible mechanism underlying TE activation in the VC is active DNA demethylation. DNA  
79 methylation in plants occurs on cytosines in three sequence contexts: CG, CHG and CHH (H=A,  
80 C or T). Approximately ten thousand loci – predominantly TEs – are hypomethylated in the  
81 VC, primarily in the CG context and to a lesser extent in the CHG/H contexts (Calarco et al.,  
82 2012; Ibarra et al., 2012). Hypomethylation in the VC is caused by a DNA glycosylase called  
83 DEMETER (DME) (Ibarra et al., 2012). DME demethylates DNA via direct excision of  
84 methylated cytosine, and its expression is strictly confined to the VC and its female counterpart,  
85 the central cell, during sexual reproduction (Choi et al., 2002; Schoft et al., 2011). DME  
86 demethylation may therefore cause TE transcription in the VC, however, this hypothesis has  
87 not been tested.

88 Another plausible mechanism for epigenetic TE activation is chromatin decondensation (Feng,  
89 Zilberman, & Dickinson, 2013). Drastic reprogramming of histone variants and histone  
90 modifications occurs during both male and female gametogenesis, rendering the gametes and  
91 companion cells with radically different chromatin states (Baroux, Raissig, & Grossniklaus,  
92 2011; Borg & Berger, 2015). For example, centromeric repeats, which are condensed in sperm  
93 and other cell types, are decondensed in the VC, accompanied by the depletion of centromeric  
94 histone H3 (Ingouff et al., 2010; Merai et al., 2014; Schoft et al., 2009). Chromocenters, which  
95 are comprised of condensed pericentromeric heterochromatin and rDNA repeats

96 (Chandrasekhara, Mohannath, Blevins, Pontvianne, & Pikaard, 2016; Fransz, de Jong, Lysak,  
97 Castiglione, & Schubert, 2002; Tessadori, van Driel, & Fransz, 2004), are observed in sperm  
98 nuclei but absent in the VC nucleus, suggesting that pericentromeric heterochromatin is  
99 decondensed in the VC (Baroux et al., 2011; Ingouff et al., 2010; Schoft et al., 2009).  
100 Heterochromatin decondensation in the VC is proposed to promote rDNA transcription that  
101 empowers pollen tube growth (Merai et al., 2014). However, the cause of VC heterochromatin  
102 decondensation remains unclear.

103 Our previous work showed that histone H1, which binds to the nucleosome surface and the  
104 linker DNA between two adjacent nucleosomes (Fyodorov, Zhou, Skoultchi, & Bai, 2018), is  
105 depleted in *Arabidopsis* VC nuclei (Hsieh et al., 2016). H1 depletion in the VC has also been  
106 observed in a distantly related lily species (Tanaka, Ono, & Fukuda, 1998), suggesting a  
107 conserved phenomenon in flowering plants. In *Drosophila* and mouse embryonic stem cells,  
108 H1 has been shown to contribute to heterochromatin condensation (Cao et al., 2013; Lu et al.,  
109 2009). H1 is also more abundant in heterochromatin than euchromatin in *Arabidopsis* (Ascenzi  
110 & Gantt, 1999; Rutowicz et al., 2015). However, it is unknown whether H1 participates in  
111 heterochromatin condensation in plant cells, and specifically whether the lack of H1 contributes  
112 to heterochromatin decondensation in the VC.

113 Whether and how the depletion of H1 in the VC contributes to TE derepression is also unclear.  
114 A recent study pointed to an intriguing link between H1 and DME. In the central cell, the  
115 histone chaperone FACT (facilitates chromatin transactions) is required for DME-directed  
116 DNA demethylation in heterochromatic TEs, and this requirement is dependent on H1 (Frost  
117 et al., 2018). However, DME activity in the VC is independent of FACT (Frost et al., 2018).  
118 One attractive hypothesis is that the lack of H1 in the VC causes heterochromatin  
119 decondensation and thereby contributes to the independence of DME from FACT. H1 depletion

120 may therefore participate in VC TE activation by promoting DME-directed demethylation.  
121 Additionally, H1 depletion may activate TE transcription independently of DNA methylation,  
122 as shown in *Drosophila* where DNA methylation is absent (Iwasaki et al., 2016; Lu et al., 2013;  
123 Vujatovic et al., 2012; Zemach, McDaniel, Silva, & Zilberman, 2010; G. Q. Zhang et al., 2015).

124 In this study, we identify heterochromatic TEs that are epigenetically activated in *Arabidopsis*  
125 VCs. We demonstrate that these TEs are typically subject to DME-directed demethylation at  
126 the transcriptional start site (TSS), which is at least partially permitted by the depletion of H1.  
127 However, we find that loss of H1 activates some TEs without altering DNA methylation. We  
128 also show that developmental depletion of H1 decondenses heterochromatin in late  
129 microspores and is important for pollen fertility. Our results demonstrate that H1 condenses  
130 heterochromatin in plants and maintains genome stability by silencing TEs via methylation-  
131 dependent and -independent mechanisms.

## 132 **Results**

### 133 **Heterochromatic transposons are preferentially expressed in the vegetative cell**

134 To measure the extent of TE activation in the VC, we performed RNA-seq using mature pollen  
135 grains, followed by the annotation of gene and TE transcripts using Mikado and the TAIR10  
136 annotation (Venturini, Caim, Kaithakottil, Mapleson, & Swarbreck, 2018). We identified 114  
137 TEs that are transcribed at significantly higher levels in pollen than rosette leaves (fold change >  
138 2;  $p < 0.05$ , likelihood ratio test), and hence likely to be specifically activated in the VC (*Figure*  
139 *1—source data 1*) (Slotkin et al., 2009).

140 The VC-activated TEs are primarily located in pericentromeric regions and exhibit features of  
141 heterochromatic TEs, such as being long and GC rich (Frost et al., 2018) (*Figure 1A,B, Figure*  
142 *1—figure supplement 1A*). As is typical of heterochromatic TEs (Zemach et al., 2013), VC-

143 activated TEs are significantly enriched in dimethylation of histone H3 on lysine 9 (H3K9me2)  
144 in somatic tissues, and are significantly depleted of euchromatin-associated modifications  
145 (*Figure 1B, Figure 1—figure supplement 1B*). VC-activated TEs encompass diverse TE  
146 families, among which MuDR DNA transposons and Gypsy LTR-retrotransposons are  
147 significantly overrepresented ( $p < 10^{-9}$  and 0.01, respectively, Fisher's exact test; *Figure 1C*).

#### 148 **Transposon derepression in the VC is caused by DME-directed DNA demethylation**

149 To assess whether TE activation in the VC is caused by DME-mediated DNA demethylation,  
150 we examined DNA methylation in VC and sperm at the 114 activated TEs. We found that these  
151 TEs have substantially lower CG methylation in the VC than in sperm at and near the TSS  
152 (*Figure 1D,E, Figure 1—figure supplement 1D*), indicative of DME activity. Because TEs tend  
153 to be flanked by repeats (Joly-Lopez & Bureau, 2018), the transcriptional termination site (TTS)  
154 regions of activated TEs also tend to be hypomethylated in the VC (*Figure 1D,E, Figure 1—*  
155 *figure supplement 1D*). Examination of DNA methylation in VCs from *dme/+* heterozygous  
156 plants (*dme* homozygous mutants are embryonic lethal), which produce a 50:50 ratio of *dme*  
157 mutant and WT pollen, revealed partial restoration of methylation at TSS and TTS of VC-  
158 activated TEs (*Figure 1D,E*). CHG and CHH methylation is also substantially increased at the  
159 TSS (and TTS) of VC-activated TEs in *dme/+* VC (*Figure 1—figure supplement 1C*),  
160 consistent with the knowledge that DME demethylates all sequence contexts (Gehring et al.,  
161 2006; Ibarra et al., 2012).

162 Consistent with the above results, 71 of the 114 (62%) VC-activated TEs overlap VC DME  
163 targets at their TSSs (*Figure 1F, Figure 1—source data 1 & 2*). 96 out of the 114 TEs (84%)  
164 have VC DME targets within 500 bp of the TSS (*Figure 1F, Figure 1—source data 1*). As  
165 DNA methylation at/near the TSS has been well-demonstrated to suppress the transcription of  
166 genes and TEs in plants and animals (Barau et al., 2016; Eichten et al., 2012; Hollister & Gaut,



167 2009; Manakov et al., 2015; Meng et al., 2016), our results indicate that DME-directed  
168 demethylation is a major mechanism of TE activation in the VC.

### 169 **Vegetative-cell-expressed H1 impedes DME from accessing heterochromatic transposons**

170 We next tested our hypothesis that the lack of histone H1 in the VC (Hsieh et al., 2016) allows  
171 heterochromatin to be accessible by DME. We first examined the developmental timing of H1  
172 depletion during microspore and pollen development using GFP translational fusion lines  
173 (Hsieh et al., 2016; She et al., 2013). There are three H1 homologs in *Arabidopsis*, with H1.1  
174 and H1.2 encoding the canonical H1 proteins, and H1.3 expressed at a much lower level and  
175 induced by stress (Rutowicz et al., 2015). H1.1- and H1.2- GFP reporters exhibit the same  
176 expression pattern: present in early microspore nucleus but absent in the late microspore stage,  
177 and remaining absent in the VC nucleus while present in the generative cell and subsequent  
178 sperm nuclei (*Figure 2A*). H1.3 is not detectable in either microspore or pollen (*Figure 2A*).  
179 These results are consistent with our previous observations, confirming that H1 is absent in the  
180 VC (Hsieh et al., 2016), and demonstrating that H1 depletion begins at the late microspore  
181 stage.

182 To understand how H1 affects DME activity, we ectopically expressed H1 in the VC. To ensure  
183 H1 incorporation into VC chromatin, we used the *pLAT52* promoter, which is expressed from  
184 the late microspore stage immediately prior to Pollen Mitosis 1, and is progressively  
185 upregulated in VC during later stages of pollen development (Eady, Lindsey, & Twell, 1994;  
186 Grant-Downton et al., 2013). Using *pLAT52* to drive the expression of H1.1 tagged with mRFP  
187 (simplified as *pVC::H1*), we observed continuous H1-mRFP signal in the VC at the bicellular  
188 and tricellular pollen stages, while the signal was undetectable in the generative cell and sperm  
189 (*Figure 2B*). H1-mRFP signal was also undetectable in late microspores (*Figure 2B*), probably  
190 due to the low activity of *pLAT52* at this stage (Eady et al., 1994). Notably, we found H1

191 expression in VC leads to shortened siliques and a substantial proportion of malformed pollen  
192 (*Figure 2—figure supplement 1A-C*), suggesting the depletion of H1 in the VC is important for  
193 pollen fertility.

194 To evaluate the effect of VC-expressed H1 on DNA methylation, we obtained genome-wide  
195 methylation profiles for VC nuclei from a strong *pVC::H1* line (#2; *Figure 2B*) and WT via  
196 fluorescence-activated cell sorting (FACS) followed by bisulfite sequencing (Supplementary  
197 file 1). CG methylation in the VC of *pVC::H1* plants is largely similar to that of WT, except  
198 for a slight increase in TE methylation (*Figure 2C, Figure 2—figure supplement 2A*).  
199 Consistently, the frequency distribution of CG methylation differences between VCs of  
200 *pVC::H1* and WT at loci that are not DME targets peaks near zero, showing almost no global  
201 difference (*Figure 2D*). However, a substantial proportion of loci that are targeted by DME  
202 show hypermethylation in *pVC::H1* VC (*Figure 2D*). DME targets also show preferential  
203 hypermethylation in CHG and CHH contexts in the VC of *pVC::H1* (*Figure 2—figure*  
204 *supplement 2B-C*). These results indicate that H1 expression in the VC specifically impedes  
205 DME activity.

206 Across the genome, we found 2964 differentially methylated regions (DMRs) that are  
207 significantly CG hypermethylated in the VC of *pVC::H1* plants (referred to as H1 hyperDMRs  
208 hereafter; ranging from 101 to 2155 nt in length, 280 nt on average; *Figure 2—source data 1*).  
209 Most of the H1 hyperDMRs (1618, 55%) overlap DME targets in the VC (*Figure 2—source*  
210 *data 1*), and H1 hyperDMRs exhibit strong hypomethylation in WT VCs, with 81.4% (2412  
211 sites) having significantly more CG methylation in sperm than VC ( $p < 0.001$ , Fisher's exact  
212 test), indicating that most H1 hyperDMRs are DME targets (*Figure 2E-H*).

213 Our results demonstrate that H1 hyperDMRs are primarily caused by the inhibition of DME.  
214 However, only 3066 out of 11896 (26%) VC DME targets have significantly more CG

215 methylation in the VC of *pVC::H1* than WT ( $p < 0.001$ , Fisher's exact test; *Figure 1—source*  
216 *data 2*), indicating that VC-expressed H1 impedes DME at a minority of its genomic targets.  
217 These H1-impeded DME targets are heterochromatic, significantly enriched in H3K9me2  
218 compared with H1-independent DME targets (*Figure 2I*). To further examine the link with  
219 heterochromatin, we aligned all VC DME target loci at the most hypomethylated cytosine, and  
220 separated them into five groups by H3K9me2 levels (*Figure 2J*). *pVC::H1*-induced  
221 hypermethylation peaks where DME-mediated hypomethylation peaks, but is apparent only in  
222 the most heterochromatic group (highest H3K9me2) of DME target loci (*Figure 2J*). Taken  
223 together, our results demonstrate that developmental removal of H1 from the VC allows DME  
224 to access heterochromatin.

### 225 **H1 represses transposons via methylation-dependent and independent mechanisms**

226 Given the importance of H1 removal for DME-directed DNA demethylation, we investigated  
227 the contribution of H1 to TE activation in the VC. RNA-seq was performed using pollen from  
228 the *pVC::H1* line (#2), which showed strong H1 expression in VC (*Figures 2B and 3A*). 47 out  
229 of 114 (41%) VC-activated TEs show significant differential expression (fold change  $> 2$ ;  
230  $p < 0.05$ , likelihood ratio test) due to H1 expression in VC (*Figure 3B*). Among these  
231 differentially expressed TEs, the overwhelming majority (46; 98%) are repressed (*Figure 3B,C*,  
232 *Figure 1—source data 1*). In contrast to the effect of H1 on TE transcription, a much smaller  
233 fraction of genes (3%; 89 out of 2845 pollen-expressed genes) is differentially expressed (fold  
234 change  $> 2$ ;  $p < 0.05$ , likelihood ratio test) between *pVC::H1* and WT (*Figure 3D*). These data  
235 indicate that ectopic expression of H1 in the VC preferentially represses TEs.

236 Quantitative RT-PCR validated our RNA-seq results and confirmed the strong suppression of  
237 TEs in *pVC::H1* (*Figure 3E*). Taking advantage of a *pVC::H1* line #7 with weaker H1  
238 expression in pollen (*Figure 3A*), we found H1 represses TE expression in a dosage-dependent

239 manner; as TEs are suppressed to a lesser extent in line #7 compared to the strong line #2  
240 (*Figure 3E*). H1-repressed TEs in the VC are predominantly localized to pericentromeric  
241 regions and are overrepresented for LTR retrotransposons, including Gypsy and Copia  
242 elements (*Figure 3F-H*). Compared to other VC-activated TEs, the H1-repressed TEs are  
243 significantly longer and enriched for H3K9me2 and H1 in somatic tissues (*Figure 3G*),  
244 consistent with the observation that H1 precludes DME access to heterochromatin.

245 In support of the hypothesis that H1 represses VC TE expression by blocking DME, 18 of 46  
246 H1-repressed TEs show significant increase of DNA methylation in at least one sequence  
247 context within 300 bp of the TSS in *pVC::H1* ( $p < 0.001$ , Fisher's exact test; *Figure 4A,B*). Six  
248 more TEs overlap a DME target, which is hypermethylated in *pVC::H1*, within 1 kb of the TSS,  
249 and hence may also be suppressed by DME inhibition. However, 22 TEs do not overlap any  
250 H1 hyperDMRs within 1 kb of the TSS (*Figure 4A*, marked by asterisks in the lower panel),  
251 indicating that their suppression by H1 is not mediated by DNA methylation. Of these, 16 TEs  
252 overlap DME targets within 1 kb of TSS. DME maintains access to these TEs in the presence  
253 of H1, suggesting their VC demethylation does not rely on the depletion of H1 and their  
254 repression in *pVC::H1* is DME-independent; exemplified by AT3TE60310 (*Figure 4C*). Our  
255 results demonstrate that H1 overexpression in the VC represses heterochromatic TEs via both  
256 DNA methylation-dependent and independent mechanisms.

## 257 **Depletion of H1 decondenses heterochromatin during male gametogenesis**

258 H1 depletion and TE activation in the VC are accompanied by loss of cytologically detectable  
259 heterochromatin (Baroux et al., 2011; Ingouff et al., 2010; Schoft et al., 2009). We therefore  
260 tested whether H1 contributes to heterochromatin condensation in plant cells. Immunostaining  
261 of leaf nuclei showed that H1 co-localizes with H3K9me2 in highly-compacted  
262 heterochromatic foci, known as chromocenters (*Figure 5A*). Furthermore, we found that

263 chromocenters become dispersed in the nuclei of *h1* mutant rosette leaves (*Figure 5B*). These  
264 observations demonstrate that H1 is required for heterochromatin condensation in plants.

265 We then examined whether ectopic H1 expression can condense the heterochromatin in VC  
266 nuclei. Consistent with previous observations (Baroux et al., 2011; Ingouff et al., 2010; Schoft  
267 et al., 2009), no condensed chromocenters were detected in WT VC (*Figure 5C*). *pVC::H1* VC  
268 also showed no obvious chromocenters (*Figure 2B*). This suggests either that H1 expression is  
269 not strong enough in *pVC::H1*, or other factors are involved in heterochromatin decondensation  
270 in the VC.

271 Heterochromatin decondensation during male gametogenesis seems to be gradual:  
272 chromocenters are observed at early microspore stage, but become dispersed in late microspore  
273 stage, when H1 is depleted (*Figures 2A* and *5C*). We observed strong and weak chromocenters  
274 in 27% and 59%, respectively, of late microspore nuclei, whereas no chromocenters were  
275 observed in the VC at either bicellular or tricellular pollen stage (*Figure 5C,D*). The further  
276 decondensation of VC heterochromatin after H1 depletion during the late microspore stage  
277 suggests the involvement of other factors in the VC. To test whether H1 is sufficient to induce  
278 chromatin condensation in microspores, we used the late-microspore-specific *MSP1* promoter  
279 (Honys et al., 2006) to drive H1 expression (*pMSP1::H1.1-mRFP*, short as *pMSP1::H1*). In  
280 *pMSP1::H1*, we observed strong chromocenters in the majority (68%) of late microspores  
281 (*Figure 5D*). H1 expression in *pMSP1::H1* is specific to late microspores, and co-localizes  
282 with induced chromocenters (*Figure 5E*). These results show that H1 is sufficient to promote  
283 heterochromatic foci in late microspores, thus demonstrating the causal relationship between  
284 H1 depletion and the decondensation of heterochromatin.

285

## 286 **Discussion**

287 Epigenetic reactivation of TEs in the VC of flowering plants is an intriguing phenomenon,  
288 which is important not only for understanding sexual reproduction, but also for elucidating  
289 epigenetic silencing mechanisms. Here we show that *Arabidopsis* VC-activated TEs are  
290 heterochromatic, and mostly subject to DME-directed demethylation at their TSS (*Figure 1F*).  
291 Given the well-demonstrated role of DNA methylation at the TSS for transcriptional  
292 suppression (Barau et al., 2016; Eichten et al., 2012; Hollister & Gaut, 2009; Manakov et al.,  
293 2015; Meng et al., 2016), our data demonstrate that DME-mediated demethylation in the VC  
294 is the primary cause of TE activation. As DNA demethylation of TEs during reproduction also  
295 occurs in rice and maize (Park et al., 2016; Rodrigues et al., 2013; M. Zhang et al., 2014),  
296 species that diverged from *Arabidopsis* more than 150 million years ago (Chaw, Chang, Chen,  
297 & Li, 2004), our results suggest that TE activation in the VC is prevalent among flowering  
298 plants.

299 DME demethylates about ten thousand loci in the VC and central cell, respectively, however,  
300 only half of these loci overlap (Ibarra et al., 2012). It was unclear why DME targets differ in  
301 these cell types, but differences in chromatin configuration have been postulated to contribute  
302 (Feng et al., 2013). Our finding that the access of DME to heterochromatic TEs in the VC is  
303 permitted by the lack of H1 supports this idea. H1 is presumably present in the central cell  
304 (Frost et al., 2018) but is absent in the VC (Hsieh et al., 2016), thus rendering heterochromatic  
305 TEs more accessible in the VC. Differential distribution of other factors in the VC and central  
306 cell, such as histone variant H3.1 (Borg & Berger, 2015; Ingouff et al., 2010), may also affect  
307 DME targeting. Consistently, FACT is required for DME activity in the central cell at many  
308 loci even in the absence of H1, whereas DME is entirely independent of FACT in the VC (Frost  
309 et al., 2018), suggesting the presence of impeding factor(s) other than H1 in the central cell.

310 With distinct chromatin architectures, the vegetative and central cells are excellent systems for  
311 understanding how chromatin regulates DNA demethylation.

312 Our finding that histone H1 affects DME activity adds to the emerging picture of H1 as an  
313 important and complex regulator of eukaryotic DNA methylation. H1 depletion causes local  
314 hypomethylation in mouse cells (Fan et al., 2005) and extensive hypermethylation in the fungi  
315 *Ascobolus immersus* (Barra, Rhounim, Rossignol, & Faugeron, 2000) and *Neurospora crassa*  
316 (Seymour et al., 2016). In *Arabidopsis*, loss of H1 causes global heterochromatic  
317 hypermethylation in all sequence contexts by allowing greater access of DNA  
318 methyltransferases (Lyons & Zilberman, 2017; Zemach et al., 2013). Our results suggest that  
319 H1 may also influence DME-homologous demethylases that control methylation in somatic  
320 tissues (He et al., 2011). By regulating both methylation and demethylation, H1 may serve as  
321 an integrator of methylation pathways that tunes methylation up or down depending on the  
322 locus.

323 Our data also indicate that the regulatory functions of H1 extend beyond DNA methylation in  
324 plants. Activated TEs in the VC can be categorized into four groups, based on the mechanism  
325 of their activation (*Figure 6*). TEs in Group I are the least heterochromatic and their activation  
326 is dependent on DME but not H1 (*Figures 3D and 6*). Group II comprises TEs in which H1  
327 absence is required for DME demethylation and activation (*Figure 6*). For TEs in Group III,  
328 H1 depletion and DME demethylation are both required for activation, but DME activity is not  
329 affected by H1 (*Figure 6*). Group IV TEs are activated by H1 depletion and are not targeted by  
330 DME (*Figure 6*). Groups III and IV demonstrate that H1 can silence TEs independently of  
331 DNA methylation. Group III also demonstrates that DNA methylation and H1 cooperate to  
332 suppress TE expression in plants. Thus, H1 regulates TEs via DNA methylation-dependent and  
333 -independent mechanisms.

334 During the ongoing arms race between TEs and their hosts, it may be difficult to determine  
335 whether TE expression represents temporary TE triumphs or is domesticated by the host to  
336 serve a function. TE activation in the VC – a cell that engulfs the male plant gametes – has  
337 been proposed as a defense strategy, which generates small RNAs that enhance TE silencing  
338 in sperm (Calarco et al., 2012; Ibarra et al., 2012; Martinez et al., 2016; Slotkin et al., 2009).  
339 However, TEs can also use companion cells as staging grounds for invasion of the gametes  
340 (Wang, Dou, Moon, Tan, & Zhang, 2018). Our demonstration that programmed DME  
341 demethylation, which is facilitated by developmental heterochromatin decondensation, is the  
342 predominant cause of VC TE activation is consistent with a defensive, host-beneficial model.  
343 Nonetheless, the alternative TE-driven model is also plausible. DME demethylation regulates  
344 genes and is important for pollen fertility (Choi et al., 2002; Ibarra et al., 2012; Schoft et al.,  
345 2011). Our data show that developmental H1 depletion is also important for pollen fertility.  
346 Therefore, at least some TEs may be hijacking an essential epigenetic reprogramming process.  
347 TE activation in the VC may facilitate both host defense and transposition, with the balance  
348 specific to each TE family and changing over evolutionary time. The effects of VC TE  
349 activation on TE proliferation in the progeny may warrant investigation, particularly in out-  
350 crossing species with aggressive TEs and in natural populations.

## 351 **Materials and Methods**

### 352 **Plant materials and growth conditions**

353 *A. thaliana* plants were grown under 16h light/ 8h dark in a growth chamber (20°C, 80%  
354 humidity). All plants used are of the Col-0 ecotype. *pH1.1::H1.1-eGFP*, *pH1.2::H1.2-eGFP*  
355 and the *h1* (*h1.1 h1.2* double) mutant lines were described previously (She et al., 2013; Zemach  
356 et al., 2013). *pLAT52::H1.1-mRFP* and *pMSP1::H1.1-mRFP* were constructed with MultiSite  
357 Gateway System into the destination vector pK7m34GW (Invitrogen). The BP clones pDONR-



358 P4-P1R-*pLAT52* and pDONR-P2R-P3-mRFP were kindly provided by Prof. David Twell  
359 (Leicester University, UK) (Eady et al., 1994). *MSP1* promoter was cloned into pDONR-P4-  
360 P1R as described previously (Honys et al., 2006). WT plants were transformed via floral dip  
361 (Clough & Bent, 1998), and T2 or T3 plants homozygous for the transgene were used in this  
362 study.

### 363 **Pollen extraction, RNA sequencing and quantitative RT-PCR**

364 Open flowers were collected for pollen isolation in Galbraith buffer (45 mM MgCl<sub>2</sub>, 30 mM  
365 sodium citrate, 20 mM MOPS, 1% Triton-X-100, pH7.0) by vortexing at 2000 rpm for 3 min.  
366 The crude fraction was filtered through a 40 µm cell strainer to remove flower parts, and  
367 subsequently centrifuged at 2600 g for 5 min to obtain pollen grains. RNA was extracted from  
368 pollen grains with RNeasy Micro Kit (Qiagen) following manufacturer's instructions. RNA-  
369 sequencing libraries were prepared using Ovation RNA-seq Systems 1-16 for Model  
370 Organisms (Nugen Technologies), and sequenced on the HiSeq 2500 (Illumina) instrument at  
371 the UC Berkeley Vincent J. Coates Genomics Sequencing Laboratory. Quantitative RT-PCR  
372 (qRT-PCR) was performed as described previously (Walker et al., 2018), and *TUA2* was used  
373 as an internal control. Primers for qRT-PCR are listed in Supplementary file 2.

### 374 **RNA-seq analysis**

375 TE transcript annotation was created using RNA-seq data from four biological replicates of  
376 pollen. Tophat2, Hisat, and STAR were used to align RNA-seq reads to the TAIR10 genome,  
377 and transcripts were assembled using CLASS2, StringTie, and Cufflinks, respectively.  
378 Assembled transcripts were selected by Mikado using default options except that the BLAST  
379 and Transdecoder steps were disabled (Venturini et al., 2018). As a result, 21381 transcripts  
380 (called superloci; GSE120519) were identified.

381 To identify VC-activated TEs, we first refined the list of superloci by selecting those  
382 overlapping with TAIR10 TE annotation. Subsequently to eliminate TE-like genes from the  
383 refined list, superloci with CG methylation less than 0.7 in rosette leaves (Stroud et al., 2014;  
384 Stroud, Greenberg, Feng, Bernatavichute, & Jacobsen, 2013) were excluded. This gave rise to  
385 an annotation of pollen TE transcripts, which was combined with TAIR10 gene annotation for  
386 Kallisto analysis (Bray, Pimentel, Melsted, & Pachter, 2016). RNA-seq data from pollen (this  
387 study) and rosette leaves (Walker et al., 2018), each including three biological replicates, were  
388 processed using Kallisto and Sleuth (Bray et al., 2016; Pimentel, Bray, Puente, Melsted, &  
389 Pachter, 2017). TEs that are transcribed at least 5 times more in pollen than leaves (with  $p <$   
390 0.05, likelihood ratio test) are considered as activated in the VC (refer to *Figure 1—source data*  
391 *1* for the list of VC-activated TEs). A total of 2845 genes were found to be expressed in pollen  
392 with TPM (transcripts per million) more than 5 in the Kallisto output (data used in *Figure 3D*).

393 To identify TEs and genes that are suppressed by H1 in the VC, we analyzed RNA-seq data  
394 from WT and *pLAT52::H1.1-mRFP line #2* (short as *pVC::H1* unless specified otherwise)  
395 pollen using Kallisto and Sleuth as described above. Significant differential expression was  
396 defined with a fold change at least 2 and a p-value less than 0.05. H1-repressed TEs were listed  
397 in *Figure 1—source data 1*.

### 398 **Whole-genome bisulfite sequencing and analysis**

399 Vegetative and sperm nuclei were isolated via FACS as described previously (Ibarra et al.,  
400 2012). Bisulfite-sequencing libraries were prepared as previously described (Walker et al.,  
401 2018). Sequencing was performed on Hiseq 2500 (Illumina) at the UC Berkeley Vincent J.  
402 Coates Genomics Sequencing Laboratory, Hiseq 4000 (Illumina) at Novogene Ltd. and  
403 Harvard University, and Nextseq 500 (Illumina) at Cambridge University Biochemistry  
404 Department and the John Innes Centre. Sequenced reads (100, 75, or 50 nt single-end) were

405 mapped to the TAIR10 reference genome, and cytosine methylation analysis was performed as  
406 previously described (Ibarra et al., 2012).

#### 407 **Identification of DME targets and H1 hyperDMRs in the VC**

408 As all CG hypomethylation in the VC in comparison to sperm is caused by DME (Ibarra et al.,  
409 2012), we identified VC DME targets via detecting CG differentially methylated regions  
410 (DMRs) that are hypermethylated in sperm in comparison to the VC. DMRs were identified  
411 first by using MethPipe (settings:  $p = 0.05$  and  $\text{bin} = 100$ ) (Song et al., 2013), and subsequently  
412 retained if the fractional CG methylation across the whole DMR was at least 0.2 higher in  
413 sperm than the VC. The refined DMRs were merged to generate larger DMRs if they occurred  
414 within 300 bp. Finally, merged DMRs were retained if they cover at least 100 bp, and the  
415 fractional CG methylation across the whole DMR was significantly (Fisher's exact test  $p <$   
416  $0.01$ ) and substantially ( $>0.2$ ) higher in sperm than the VC. This resulted in the identification  
417 of 11896 VC DME targets (*Figure 1—source data 2*).

418 H1 hyperDMRs were identified using the same criteria, except comparing CG methylation in  
419 VCs from *pVC::H1* and WT. In total, 2964 H1 hyperDMRs were identified (*Figure 2—source*  
420 *data 1*).

#### 421 **Box plots**

422 Box plots compare the enrichment of genomic or chromatin features among TEs (*Figure 1B,*  
423 *3G, Figure 1—figure supplement 1B*) or VC DME targets (*Figure 2I*) as described in  
424 corresponding figure legends. ChIP-seq data for H3K9me2 (Stroud et al., 2014), and ChIP-  
425 chip data for H1 (Rutowicz et al., 2015), H3K27me3 (Kim, Lee, Eshed-Williams, Zilberman,  
426 & Sung, 2012), and other histone modifications (Roudier et al., 2011) were used.

## 427 **Density plots**

428 All DNA methylation kernel density plots compare fractional methylation within 50-bp  
429 windows. We used windows with at least 20 informative sequenced cytosines and fractional  
430 methylation of at least 0.5 (*Figure 2D, Figure 2—figure supplement 2*) or 0.7 (*Figure 2E*) for  
431 CG context, and 0.4 and 0.1 for CHG and CHH context, respectively, in at least one of the  
432 samples being compared.

## 433 **Meta analysis (ends analysis)**

434 Ends analysis for TEs and genes was performed as described previously (Ibarra et al., 2012).  
435 Similarly, ends analysis of TE transcripts was performed using the annotation of VC-activated  
436 TEs described above (*Figure 1—source data 1*). DNA methylation data from (Ibarra et al.,  
437 2012) was used.

438 In *Figure 2J*, DME sites were aligned at the most demethylated cytosine, and average CG  
439 methylation levels for each 10-bp interval at both sides were plotted. To identify individual  
440 hypomethylation sites created by DME, we first obtained the 50-bp windows with a CG  
441 methylation difference larger than 0.5 between sperm and VC (sperm – VC > 0.5 and Fisher's  
442 exact test  $p < 0.001$ ). Windows were then merged if they occurred within 200 bp. Merged  
443 windows were retained for further analysis if the fractional CG methylation across the whole  
444 site was 0.2 greater in sperm than VC (sperm – VC > 0.2 and Fisher's exact test  $p < 0.0001$ ).  
445 This resulted in 13610 DME sites, which were separated into five groups according to  
446 H3K9me2 level (Stroud et al., 2014): < 2.5, 2.5-4.3, 4.3-6.5, 6.5-10.5, and > 10.5 (*Figure 2J*).  
447 The most demethylated cytosine within each site was identified if it had the greatest differential  
448 methylation in sperm than VC among cytosines in the CG context (sperm – VC > 0.2, and  
449 Fisher's exact test  $p < 0.001$ ) and was sequenced at least 10 times.

## 450 **DNA methylation analysis of H1-repressed TEs**

451 Differential methylation at a 600-bp region centered upon the TSS of H1-repressed TEs was  
452 calculated between VCs of *pVC::H1* and WT (*Figure 4A*). TEs whose differential methylation  
453 is significant (Fisher's exact test  $p < 0.001$ ) and larger than 0.2 (in CG context), 0.1 (in CHG  
454 context), or 0.05 (in CHH context) are illustrated in the upper panel in *Figure 4A*.

## 455 **Confocal and scanning electron microscopy**

456 Microspores and pollen were isolated as described previously (Borges et al., 2012), stained  
457 with Hoechst or DAPI, and examined under a Leica SP8 confocal microscope. Scanning  
458 electron microscopy was performed on a Zeiss Supra 55 VP FEG.

## 459 **Immunofluorescence**

460 Immunofluorescence was performed as described previously with small modifications  
461 (Yelagandula et al., 2014). Rosette leaves from 3-week-old plants were fixed in TRIS buffer  
462 with 4% paraformaldehyde (10 mM Tris-HCl pH 7.5, 10 mM EDTA, 100 mM NaCl) for 20  
463 min. After being washed with TRIS buffer twice, the fixed leaves were chopped with razor  
464 blades in 1 mL of lysis buffer (15 mM Tris pH 7.5, 2 mM EDTA, 0.5 mM spermine, 80 mM  
465 KCl, 20 mM NaCl, 0.1% Triton X-100) and filtered through a 35  $\mu$ m cell strainer. Nuclei were  
466 pelleted via centrifugation at 500 g for 3 min and resuspended in 100  $\mu$ L of lysis buffer. Next,  
467 10  $\mu$ L was spotted onto coverslips, air-dried, and post-fixed in PBS with 4% paraformaldehyde  
468 for 30 min. After being washed with PBS twice, coverslips were incubated in blocking buffer  
469 (PBS with 1% BSA) at 37°C for 30 min and then incubated in blocking buffer with primary  
470 antibodies at 4°C overnight (Mouse anti-H3K9me2 Abcam ab1220, 1:100; Rabbit anti-GFP  
471 Abcam ab290, 1:100). After being washed with PBS three times, coverslips were incubated in  
472 PBS with secondary antibodies at 37°C for 30 min, and then washed with PBS three times

473 again before being counterstained and mounted in Vectashield mounting media with DAPI  
474 (Vector H-1200).

## 475 **Acknowledgements**

476 We thank David Twell for the pDONR-P4-P1R-pLAT52 and pDONR-P2R-P3-mRFP vectors,  
477 the John Innes Centre Bioimaging Facility (Elaine Barclay and Grant Calder) for their  
478 assistance with microscopy, and the Norwich BioScience Institute Partnership Computing  
479 infrastructure for Science Group for High Performance Computing resources. This work was  
480 funded by a Biotechnology and Biological Sciences Research Council (BBSRC) David Phillips  
481 Fellowship (BBL0250431) and Grant to Exceptional Researchers by the Gatsby Charitable  
482 Foundation to X.F.

## 483 **Author contributions**

484 S.H. and X.F. designed the study and wrote the manuscript, S.H. and J.Z. performed the  
485 experiments, and S.H. and M.V. analyzed the data.

## 486 **Author information**

487 Sequencing data have been deposited in GEO (GSE120519). The authors declare no competing  
488 financial interests. Correspondence and requests for materials should be addressed to X.F.  
489 ([xiaoqi.feng@jic.ac.uk](mailto:xiaoqi.feng@jic.ac.uk)).

490

## 491 **References**

- 492 Anwar, S. L., Wulaningsih, W., & Lehmann, U. (2017). Transposable Elements in Human  
493 Cancer: Causes and Consequences of Deregulation. *International Journal of Molecular*  
494 *Sciences*, 18(5). doi:10.3390/ijms18050974
- 495 Ascenzi, R., & Gantt, J. S. (1999). Subnuclear distribution of the entire complement of linker  
496 histone variants in *Arabidopsis thaliana*. *Chromosoma*, 108(6), 345-355.  
497 doi:10.1007/S004120050386
- 498 Barau, J., Teissandier, A., Zamudio, N., Roy, S., Nalesso, V., Herault, Y., . . . Bourc'his, D.  
499 (2016). The DNA methyltransferase DNMT3C protects male germ cells from transposon  
500 activity. *Science*, 354(6314), 909-912. doi:10.1126/science.aah5143
- 501 Baroux, C., Raissig, M. T., & Grossniklaus, U. (2011). Epigenetic regulation and  
502 reprogramming during gamete formation in plants. *Current Opinion in Genetics &*  
503 *Development*, 21(2), 124-133. doi:10.1016/j.gde.2011.01.017
- 504 Barra, J. L., Rhounim, L., Rossignol, J. L., & Faugeron, G. (2000). Histone H1 is dispensable  
505 for methylation-associated gene silencing in *Ascobolus immersus* and essential for long life  
506 span. *Molecular and Cellular Biology*, 20(1), 61-69. doi:Doi 10.1128/Mcb.20.1.61-69.2000
- 507 Berger, F., & Twell, D. (2011). Germline specification and function in plants. *Annual Review*  
508 *of Plant Biology*, Vol 62, 62, 461-484. doi:10.1146/annurev-arplant-042110-103824
- 509 Borg, M., & Berger, F. (2015). Chromatin remodelling during male gametophyte development.  
510 *Plant Journal*, 83(1), 177-188. doi:10.1111/tpj.12856
- 511 Borges, F., Gardner, R., Lopes, T., Calarco, J. P., Boavida, L. C., Slotkin, R. K., . . . Becker, J.  
512 D. (2012). FACS-based purification of *Arabidopsis* microspores, sperm cells and vegetative  
513 nuclei. *Plant Methods*, 8. doi:10.1186/1746-4811-8-44
- 514 Bray, N. L., Pimentel, H., Melsted, P., & Pachter, L. (2016). Near-optimal probabilistic RNA-  
515 seq quantification. *Nature Biotechnology*, 34(5), 525-527. doi:10.1038/nbt.3519
- 516 Calarco, J. P., Borges, F., Donoghue, M. T. A., Van Ex, F., Jullien, P. E., Lopes, T., . . .  
517 Martienssen, R. A. (2012). Reprogramming of DNA Methylation in Pollen Guides Epigenetic  
518 Inheritance via Small RNA. *Cell*, 151(1), 194-205. doi:10.1016/j.cell.2012.09.001
- 519 Cao, K., Lailler, N., Zhang, Y., Kumar, A., Uppal, K., Liu, Z., . . . Fan, Y. (2013). High-  
520 resolution mapping of h1 linker histone variants in embryonic stem cells. *Plos Genetics*, 9(4),  
521 e1003417.
- 522 Chandrasekhara, C., Mohannath, G., Blevins, T., Pontvianne, F., & Pikaard, C. S. (2016).  
523 Chromosome-specific NOR inactivation explains selective rRNA gene silencing and dosage  
524 control in *Arabidopsis*. *Genes & Development*, 30(2), 177-190. doi:10.1101/gad.273755.115

- 525 Chaw, S. M., Chang, C. C., Chen, H. L., & Li, W. H. (2004). Dating the monocot-dicot  
526 divergence and the origin of core eudicots using whole chloroplast genomes. *Journal of*  
527 *Molecular Evolution*, 58(4), 424-441. doi:10.1007/s00239-003-2564-9
- 528 Choi, Y. H., Gehring, M., Johnson, L., Hannon, M., Harada, J. J., Goldberg, R. B., . . . Fischer,  
529 R. L. (2002). DEMETER, a DNA glycosylase domain protein, is required for endosperm gene  
530 imprinting and seed viability in Arabidopsis. *Cell*, 110(1), 33-42. doi:10.1016/S0092-  
531 8674(02)00807-3
- 532 Clough, S. J., & Bent, A. F. (1998). Floral dip: a simplified method for Agrobacterium-  
533 mediated transformation of Arabidopsis thaliana. *Plant Journal*, 16(6), 735-743. doi:10.1046/j.1365-3113x.1998.00343.x
- 535 Coufal, N. G., Garcia-Perez, J. L., Peng, G. E., Yeo, G. W., Mu, Y. L., Lovci, M. T., . . . Gage,  
536 F. H. (2009). L1 retrotransposition in human neural progenitor cells. *Nature*, 460(7259), 1127-  
537 1131. doi:10.1038/nature08248
- 538 Eady, C., Lindsey, K., & Twell, D. (1994). Differential Activation and Conserved Vegetative  
539 Cell-Specific Activity of a Late Pollen Promoter in Species with Bicellular and Tricellular  
540 Pollen. *Plant Journal*, 5(4), 543-550. doi:10.1046/j.1365-3113X.1994.05040543.x
- 541 Eichten, S. R., Ellis, N. A., Makarevitch, I., Yeh, C. T., Gent, J. I., Guo, L., . . . Springer, N.  
542 M. (2012). Spreading of Heterochromatin Is Limited to Specific Families of Maize  
543 Retrotransposons. *Plos Genetics*, 8(12). doi:10.1371/journal.pgen.1003127
- 544 Fadloun, A., Le Gras, S., Jost, B., Ziegler-Birling, C., Takahashi, H., Gorab, E., . . . Torres-  
545 Padilla, M. E. (2013). Chromatin signatures and retrotransposon profiling in mouse embryos  
546 reveal regulation of LINE-1 by RNA. *Nature Structural & Molecular Biology*, 20(3), 332-338.  
547 doi:10.1038/nsmb.2495
- 548 Fan, Y. H., Nikitina, T., Zhao, J., Fleury, T. J., Bhattacharyya, R., Bouhassira, E. E., . . .  
549 Skoultschi, A. I. (2005). Histone H1 depletion in mammals alters global chromatin structure but  
550 causes specific changes in gene regulation. *Cell*, 123(7), 1199-1212.  
551 doi:10.1016/j.cell.2005.10.028
- 552 Feng, X. Q., Zilberman, D., & Dickinson, H. (2013). A Conversation across Generations:  
553 Soma-Germ Cell Crosstalk in Plants. *Developmental Cell*, 24(3), 215-225.  
554 doi:10.1016/j.devcel.2013.01.014
- 555 Fransz, P., de Jong, J. H., Lysak, M., Castiglione, M. R., & Schubert, I. (2002). Interphase  
556 chromosomes in Arabidopsis are organized as well defined chromocenters from which  
557 euchromatin loops emanate. *Proceedings of the National Academy of Sciences of the United*  
558 *States of America*, 99(22), 14584-14589. doi:10.1073/pnas.212325299
- 559 Frost, J. M., Kim, M. Y., Park, G. T., Hsieh, P. H., Nakamura, M., Lin, S. J. H., . . . Fischer, R.  
560 L. (2018). FACT complex is required for DNA demethylation at heterochromatin during  
561 reproduction in Arabidopsis. *Proceedings of the National Academy of Sciences of the United*  
562 *States of America*, 115(20), E4720-E4729.



- 563 Fyodorov, D. V., Zhou, B. R., Skoultchi, A. I., & Bai, Y. W. (2018). Emerging roles of linker  
564 histones in regulating chromatin structure and function. *Nature Reviews Molecular Cell*  
565 *Biology*, *19*(3), 192-206. doi:10.1038/nrm.2017.94
- 566 Garcia-Perez, J. L., Widmann, T. J., & Adams, I. R. (2016). The impact of transposable  
567 elements on mammalian development. *Development*, *143*(22), 4101-4114.  
568 doi:10.1242/dev.132639
- 569 Gehring, M., Huh, J. H., Hsieh, T. F., Penterman, J., Choi, Y., Harada, J. J., . . . Fischer, R. L.  
570 (2006). DEMETER DNA glycosylase establishes MEDEA polycomb gene self-imprinting by  
571 allele-specific demethylation. *Cell*, *124*(3), 495-506. doi:10.1016/j.cell.2005.12.034
- 572 Grant-Downton, R., Kourmpetli, S., Hafidh, S., Khatab, H., Le Trionnaire, G., Dickinson, H.,  
573 & Twell, D. (2013). Artificial microRNAs reveal cell-specific differences in small RNA  
574 activity in pollen. *Current Biology*, *23*(14), R599-R601. doi:10.1016/j.cub.2013.05.055
- 575 He, X. J., Chen, T. P., & Zhu, J. K. (2011). Regulation and function of DNA methylation in  
576 plants and animals. *Cell Research*, *21*(3), 442-465. doi:10.1038/cr.2011.23
- 577 Hollister, J. D., & Gaut, B. S. (2009). Epigenetic silencing of transposable elements: A trade-  
578 off between reduced transposition and deleterious effects on neighboring gene expression.  
579 *Genome Research*, *19*(8), 1419-1428. doi:10.1101/gr.091678.109
- 580 Honys, D., Oh, S. A., Renak, D., Donders, M., Solcova, B., Johnson, J. A., . . . Twell, D. (2006).  
581 Identification of microspore-active promoters that allow targeted manipulation of gene  
582 expression at early stages of microgametogenesis in Arabidopsis. *Bmc Plant Biology*, *6*.  
583 doi:10.1186/1471-2229-6-31
- 584 Hsieh, P. H., He, S. B., Buttress, T., Gao, H. B., Couchman, M., Fischer, R. L., . . . Feng, X.  
585 Q. (2016). Arabidopsis male sexual lineage exhibits more robust maintenance of CG  
586 methylation than somatic tissues. *Proceedings of the National Academy of Sciences of the*  
587 *United States of America*, *113*(52), 15132-15137. doi:10.1073/pnas.1619074114
- 588 Ibarra, C. A., Feng, X. Q., Schoft, V. K., Hsieh, T. F., Uzawa, R., Rodrigues, J. A., . . .  
589 Zilberman, D. (2012). Active DNA Demethylation in Plant Companion Cells Reinforces  
590 Transposon Methylation in Gametes. *Science*, *337*(6100), 1360-1364.  
591 doi:10.1126/science.1224839
- 592 Ingouff, M., Rademacher, S., Holec, S., Soljic, L., Xin, N., Readshaw, A., . . . Berger, F. (2010).  
593 Zygotic Resetting of the HISTONE 3 Variant Repertoire Participates in Epigenetic  
594 Reprogramming in Arabidopsis. *Current Biology*, *20*(23), 2137-2143.  
595 doi:10.1016/j.cub.2010.11.012
- 596 Iwasaki, Y. W., Murano, K., Ishizu, H., Shibuya, A., Iyoda, Y., Siomi, M. C., . . . Saito, K.  
597 (2016). Piwi Modulates Chromatin Accessibility by Regulating Multiple Factors Including  
598 Histone H1 to Repress Transposons. *Molecular Cell*, *63*(3), 408-419.  
599 doi:10.1016/j.molcel.2016.06.008
- 600 Jeddloh, J. A., Stokes, T. L., & Richards, E. J. (1999). Maintenance of genomic methylation  
601 requires a SWI2/SNF2-like protein. *Nature Genetics*, *22*(1), 94-97. doi:10.1038/8803

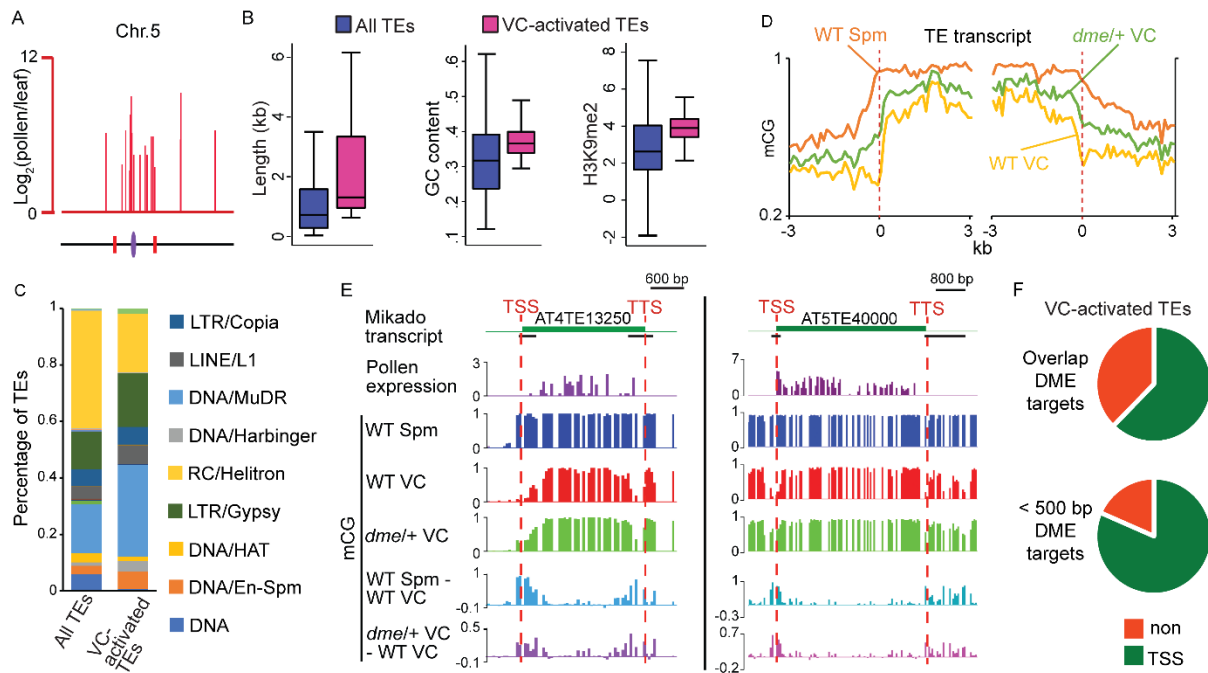
- 602 Joly-Lopez, Z., & Bureau, T. E. (2018). Exaptation of transposable element coding sequences.  
603 *Current Opinion in Genetics & Development*, *49*, 34-42. doi:10.1016/j.gde.2018.02.011
- 604 Kano, H., Godoy, I., Courtney, C., Vetter, M. R., Gerton, G. L., Ostertag, E. M., & Kazazian,  
605 H. H. (2009). L1 retrotransposition occurs mainly in embryogenesis and creates somatic  
606 mosaicism. *Genes & Development*, *23*(11), 1303-1312. doi:10.1101/gad.1803909
- 607 Kim, S. Y., Lee, J., Eshed-Williams, L., Zilberman, D., & Sung, Z. R. (2012). EMF1 and PRC2  
608 Cooperate to Repress Key Regulators of Arabidopsis Development. *Plos Genetics*, *8*(3).  
609 doi:10.1371/journal.pgen.1002512
- 610 Lander, E. S., Consortium, I. H. G. S., Linton, L. M., Birren, B., Nusbaum, C., Zody, M. C., . . .  
611 Conso, I. H. G. S. (2001). Initial sequencing and analysis of the human genome. *Nature*,  
612 *409*(6822), 860-921. doi:10.1038/35057062
- 613 Law, J. A., & Jacobsen, S. E. (2010). Establishing, maintaining and modifying DNA  
614 methylation patterns in plants and animals. *Nature Reviews Genetics*, *11*(3), 204-220.  
615 doi:10.1038/nrg2719
- 616 Lippman, Z., Gendrel, A. V., Black, M., Vaughn, M. W., Dedhia, N., McCombie, W. R., . . .  
617 Martienssen, R. (2004). Role of transposable elements in heterochromatin and epigenetic  
618 control. *Nature*, *430*(6998), 471-476. doi:10.1038/nature02651
- 619 Lu, X. W., Wontakal, S. N., Emelyanov, A. V., Morcillo, P., Konev, A. Y., Fyodorov, D. V.,  
620 & Skoultchi, A. I. (2009). Linker histone H1 is essential for Drosophila development, the  
621 establishment of pericentric heterochromatin, and a normal polytene chromosome structure.  
622 *Genes & Development*, *23*(4), 452-465. doi:10.1101/gad.1749309
- 623 Lu, X. W., Wontakal, S. N., Kavi, H., Kim, B. J., Guzzardo, P. M., Emelyanov, A. V., . . .  
624 Skoultchi, A. I. (2013). Drosophila H1 Regulates the Genetic Activity of Heterochromatin by  
625 Recruitment of Su(var)3-9. *Science*, *340*(6128), 78-81. doi:10.1126/science.1234654
- 626 Lyons, D. B., & Zilberman, D. (2017). DDM1 and Lsh remodelers allow methylation of DNA  
627 wrapped in nucleosomes. *Elife*, *6*. doi:10.7554/eLife.30674
- 628 Manakov, S. A., Pezic, D., Marinov, G. K., Pastor, W. A., Sachidanandam, R., & Aravin, A.  
629 A. (2015). MIWI2 and MILI Have Differential Effects on piRNA Biogenesis and DNA  
630 Methylation. *Cell Reports*, *12*(8), 1234-1243. doi:10.1016/j.celrep.2015.07.036
- 631 Martinez, G., Panda, K., Kohler, C., & Slotkin, R. K. (2016). Silencing in sperm cells is  
632 directed by RNA movement from the surrounding nurse cell. *Nature Plants*, *2*(4).  
633 doi:10.1038/Nplants.2016.30
- 634 Martinez, G., & Slotkin, R. K. (2012). Developmental relaxation of transposable element  
635 silencing in plants: functional or byproduct? *Current Opinion in Plant Biology*, *15*(5), 496-502.  
636 doi:10.1016/j.pbi.2012.09.001
- 637 Meng, D. Z., Dubin, M., Zhang, P., Osborne, E. J., Stegle, O., Clark, R. M., & Nordborg, M.  
638 (2016). Limited Contribution of DNA Methylation Variation to Expression Regulation in  
639 *Arabidopsis thaliana*. *Plos Genetics*, *12*(7). doi:10.1371/journal.pgen.1006141

- 640 Merai, Z., Chumak, N., Garcia-Aguilar, M., Hsieh, T. F., Nishimura, T., Schoft, V. K., . . .  
641 Tamaru, H. (2014). The AAA-ATPase molecular chaperone Cdc48/p97 disassembles  
642 sumoylated centromeres, decondenses heterochromatin, and activates ribosomal RNA genes.  
643 *Proceedings of the National Academy of Sciences of the United States of America*, *111*(45),  
644 16166-16171. doi:10.1073/pnas.1418564111
- 645 Muotri, A. R., Chu, V. T., Marchetto, M. C. N., Deng, W., Moran, J. V., & Gage, F. H. (2005).  
646 Somatic mosaicism in neuronal precursor cells mediated by L1 retrotransposition. *Nature*,  
647 *435*(7044), 903-910. doi:10.1038/nature03663
- 648 Park, K., Kim, M. Y., Vickers, M., Park, J. S., Hyun, Y., Okamoto, T., . . . Scholten, S. (2016).  
649 DNA demethylation is initiated in the central cells of Arabidopsis and rice. *Proceedings of the*  
650 *National Academy of Sciences of the United States of America*, *113*(52), 15138-15143.  
651 doi:10.1073/pnas.1619047114
- 652 Percharde, M., Lin, C. J., Yin, Y. F., Guan, J., Peixoto, G. A., Bulut-Karslioglu, A., . . .  
653 Ramalho-Santos, M. (2018). A LINE1-Nucleolin Partnership Regulates Early Development  
654 and ESC Identity. *Cell*, *174*(2), 391-+. doi:10.1016/j.cell.2018.05.043
- 655 Percharde, M., Wong, P., & Ramalho-Santos, M. (2017). Global Hypertranscription in the  
656 Mouse Embryonic Germline. *Cell Reports*, *19*(10), 1987-1996.  
657 doi:10.1016/j.celrep.2017.05.036
- 658 Pimentel, H., Bray, N. L., Puente, S., Melsted, P., & Pachter, L. (2017). Differential analysis  
659 of RNA-seq incorporating quantification uncertainty. *Nature Methods*, *14*(7), 687-+.  
660 doi:10.1038/nmeth.4324
- 661 Richardson, S. R., Gerdes, P., Gerhardt, D. J., Sanchez-Luque, F. J., Bodea, G. O., Munoz-  
662 Lopez, M., . . . Faulkner, G. J. (2017). Heritable L1 retrotransposition in the mouse primordial  
663 germline and early embryo. *Genome Research*, *27*(8), 1395-1405. doi:10.1101/gr.219022.116
- 664 Richardson, S. R., Morell, S., & Faulkner, G. J. (2014). L1 Retrotransposons and Somatic  
665 Mosaicism in the Brain. *Annual Review of Genetics*, *Vol 48*, *48*, 1-27. doi:10.1146/annurev-  
666 genet-120213-092412
- 667 Rodrigues, J. A., Ruan, R., Nishimura, T., Sharma, M. K., Sharma, R., Ronald, P. C., . . .  
668 Zilberman, D. (2013). Imprinted expression of genes and small RNA is associated with  
669 localized hypomethylation of the maternal genome in rice endosperm. *Proceedings of the*  
670 *National Academy of Sciences of the United States of America*, *110*(19), 7934-7939.  
671 doi:10.1073/pnas.1306164110
- 672 Roudier, F., Ahmed, I., Berard, C., Sarazin, A., Mary-Huard, T., Cortijo, S., . . . Colot, V.  
673 (2011). Integrative epigenomic mapping defines four main chromatin states in Arabidopsis.  
674 *Embo Journal*, *30*(10), 1928-1938. doi:10.1038/emboj.2011.103
- 675 Rutowicz, K., Puzio, M., Halibart-Puzio, J., Lirski, M., Kotlinski, M., Kroten, M. A., . . .  
676 Jerzmanowski, A. (2015). A Specialized Histone H1 Variant Is Required for Adaptive  
677 Responses to Complex Abiotic Stress and Related DNA Methylation in Arabidopsis. *Plant*  
678 *Physiology*, *169*(3), 2080-2101. doi:10.1104/pp.15.00493

- 679 Schnable, P. S., Ware, D., Fulton, R. S., Stein, J. C., Wei, F. S., Pasternak, S., . . . Wilson, R.  
680 K. (2009). The B73 Maize Genome: Complexity, Diversity, and Dynamics. *Science*, *326*(5956),  
681 1112-1115. doi:10.1126/science.1178534
- 682 Schoft, V. K., Chumak, N., Choi, Y., Hannon, M., Garcia-Aguilar, M., Machlicova, A., . . .  
683 Tamaru, H. (2011). Function of the DEMETER DNA glycosylase in the Arabidopsis thaliana  
684 male gametophyte. *Proceedings of the National Academy of Sciences of the United States of*  
685 *America*, *108*(19), 8042-8047.
- 686 Schoft, V. K., Chumak, N., Mosiolek, M., Slusarz, L., Komnenovic, V., Brownfield, L., . . .  
687 Tamaru, H. (2009). Induction of RNA-directed DNA methylation upon decondensation of  
688 constitutive heterochromatin. *Embo Reports*, *10*(9), 1015-1021. doi:10.1038/embor.2009.152
- 689 Seymour, M., Ji, L. X., Santos, A. M., Kamei, M., Sasaki, T., Basenko, E. Y., . . . Lewis, Z. A.  
690 (2016). Histone H1 Limits DNA Methylation in Neurospora crassa. *G3-Genes Genomes*  
691 *Genetics*, *6*(7), 1879-1889. doi:10.1534/g3.116.028324
- 692 She, W. J., Grimanelli, D., Rutowicz, K., Whitehead, M. W. J., Puzio, M., Kotlinski, M., . . .  
693 Baroux, C. (2013). Chromatin reprogramming during the somatic-to-reproductive cell fate  
694 transition in plants. *Development*, *140*(19), 4008-4019. doi:10.1242/dev.095034
- 695 Singer, T., McConnell, M. J., Marchetto, M. C. N., Coufal, N. G., & Gage, F. H. (2010). LINE-  
696 1 retrotransposons: mediators of somatic variation in neuronal genomes? *Trends in*  
697 *Neurosciences*, *33*(8), 345-354. doi:10.1016/j.tins.2010.04.001
- 698 Slotkin, R. K., Vaughn, M., Borges, F., Tanurdzic, M., Becker, J. D., Feijo, J. A., &  
699 Martienssen, R. A. (2009). Epigenetic reprogramming and small RNA silencing of  
700 transposable elements in pollen. *Cell*, *136*(3), 461-472. doi:10.1016/j.cell.2008.12.038
- 701 Song, Q., Decato, B., Hong, E. E., Zhou, M., Fang, F., Qu, J. H., . . . Smith, A. D. (2013). A  
702 Reference Methylome Database and Analysis Pipeline to Facilitate Integrative and  
703 Comparative Epigenomics. *Plos One*, *8*(12). doi:10.1371/journal.pone.0081148
- 704 Stroud, H., Do, T., Du, J. M., Zhong, X. H., Feng, S. H., Johnson, L., . . . Jacobsen, S. E. (2014).  
705 Non-CG methylation patterns shape the epigenetic landscape in Arabidopsis. *Nature Structural*  
706 *& Molecular Biology*, *21*(1), 64-+. doi:10.1038/nsmb.2735
- 707 Stroud, H., Greenberg, M. V. C., Feng, S. H., Bernatavichute, Y. V., & Jacobsen, S. E. (2013).  
708 Comprehensive Analysis of Silencing Mutants Reveals Complex Regulation of the  
709 Arabidopsis Methylome. *Cell*, *152*(1-2), 352-364.
- 710 Tanaka, I., Ono, K., & Fukuda, T. (1998). The developmental fate of angiosperm pollen is  
711 associated with a preferential decrease in the level of histone H1 in the vegetative nucleus.  
712 *Planta*, *206*(4), 561-569. doi:DOI 10.1007/s004250050433
- 713 Tessadori, F., van Driel, R., & Fransz, P. (2004). Cytogenetics as a tool to study gene regulation.  
714 *Trends in Plant Science*, *9*(3), 147-153. doi:10.1016/j.tplants.2004.01.008

- 715 Tsukahara, S., Kobayashi, A., Kawabe, A., Mathieu, O., Miura, A., & Kakutani, T. (2009).  
716 Bursts of retrotransposition reproduced in Arabidopsis. *Nature*, *461*(7262), 423-U125.  
717 doi:10.1038/nature08351
- 718 Venter, J. C., Adams, M. D., Myers, E. W., Li, P. W., Mural, R. J., Sutton, G. G., . . . Zhu, X.  
719 H. (2001). The sequence of the human genome. *Science*, *291*(5507), 1304-+. doi:DOI  
720 10.1126/science.1058040
- 721 Venturini, L., Caim, S., Kaithakottil, G. G., Mapleson, D. L., & Swarbreck, D. (2018).  
722 Leveraging multiple transcriptome assembly methods for improved gene structure annotation.  
723 *Gigascience*. doi:10.1093/gigascience/giy093
- 724 Vujatovic, O., Zaragoza, K., Vaquero, A., Reina, O., Bernues, J., & Azorin, F. (2012).  
725 Drosophila melanogaster linker histone dH1 is required for transposon silencing and to  
726 preserve genome integrity. *Nucleic Acids Research*, *40*(12), 5402-5414.  
727 doi:10.1093/nar/gks224
- 728 Walker, J., Gao, H. B., Zhang, J. Y., Aldridge, B., Vickers, M., Higgins, J. D., & Feng, X. Q.  
729 (2018). Sexual-lineage-specific DNA methylation regulates meiosis in Arabidopsis. *Nature*  
730 *Genetics*, *50*(1), 130-137.
- 731 Wang, L., Dou, K., Moon, S., Tan, F. J., & Zhang, Z. Z. Z. (2018). Hijacking Oogenesis  
732 Enables Massive Propagation of LINE and Retroviral Transposons. *Cell*, *174*(5), 1082-+.  
733 doi:10.1016/j.cell.2018.06.040
- 734 Wicker, T., Gundlach, H., Spannagl, M., Uauy, C., Borrill, P., Ramirez-Gonzalez, R. H., . . .  
735 Sequencing, I. W. G. (2018). Impact of transposable elements on genome structure and  
736 evolution in bread wheat. *Genome Biology*, *19*(1). doi:10.1186/s13059-018-1479-0
- 737 Yelagandula, R., Stroud, H., Holec, S., Zhou, K., Feng, S. H., Zhong, X. H., . . . Berger, F.  
738 (2014). The Histone Variant H2A. W Defines Heterochromatin and Promotes Chromatin  
739 Condensation in Arabidopsis. *Cell*, *158*(1), 98-109. doi:10.1016/j.cell.2014.06.006
- 740 Zemach, A., Kim, M. Y., Hsieh, P. H., Coleman-Derr, D., Eshed-Williams, L., Thao, K., . . .  
741 Zilberman, D. (2013). The Arabidopsis nucleosome remodeler DDM1 allows DNA  
742 methyltransferases to access H1-containing heterochromatin. *Cell*, *153*(1), 193-205.  
743 doi:10.1016/j.cell.2013.02.033
- 744 Zemach, A., McDaniel, I. E., Silva, P., & Zilberman, D. (2010). Genome-wide evolutionary  
745 analysis of eukaryotic DNA methylation. *Science*, *328*(5980), 916-919.  
746 doi:10.1126/science.1186366
- 747 Zhang, G. Q., Huang, H., Liu, D., Cheng, Y., Liu, X. L., Zhang, W. X., . . . Chen, D. H. (2015).  
748 N-6-Methyladenine DNA Modification in Drosophila. *Cell*, *161*(4), 893-906.  
749 doi:10.1016/j.cell.2015.04.018
- 750 Zhang, M., Xie, S. J., Dong, X. M., Zhao, X., Zeng, B., Chen, J., . . . Lai, J. S. (2014). Genome-  
751 wide high resolution parental-specific DNA and histone methylation maps uncover patterns of  
752 imprinting regulation in maize. *Genome Research*, *24*(1), 167-176. doi:10.1101/gr.155879.113

753 **Figure 1 with 1 supplement**



754

755 **Figure 1. VC-activated TEs are heterochromatic and demethylated by DME.** (A) Expression  
 756 and locations of VC-activated TEs along Chromosome 5. The purple ellipse and red bars indicate  
 757 the centromere and borders of pericentromeric regions, respectively. (B) Box plots showing the  
 758 length, GC content, and H3K9me2 level of TEs. Each box encloses the middle 50% of the  
 759 distribution, with the horizontal line marking the median and vertical lines marking the minimum  
 760 and maximum values that fall within 1.5 times the height of the box. Difference between the two  
 761 datasets compared for each feature is significant (Kolmogorov-Smirnov test  $p < 0.001$ ). (C)  
 762 Percentages of TEs classified by superfamily. (D) VC-activated TEs were aligned at the TSS and  
 763 TTS (dashed lines), respectively, and average CG methylation levels for each 100-bp interval were  
 764 plotted (referred to as ends analysis). (E) Snapshots demonstrating the expression ( $\text{Log}_2\text{RPKM}$ ),  
 765 absolute and differential CG methylation at two example VC-activated TEs. Black lines under TE  
 766 annotations indicate VC DME targets. (F) Pie charts illustrating percentages of VC-activated TEs  
 767 with TSS overlapping (top) or within 500 bp (bottom) of VC DME targets. Spm, sperm.

768 The following figure source data and supplement are available for Figure 1:

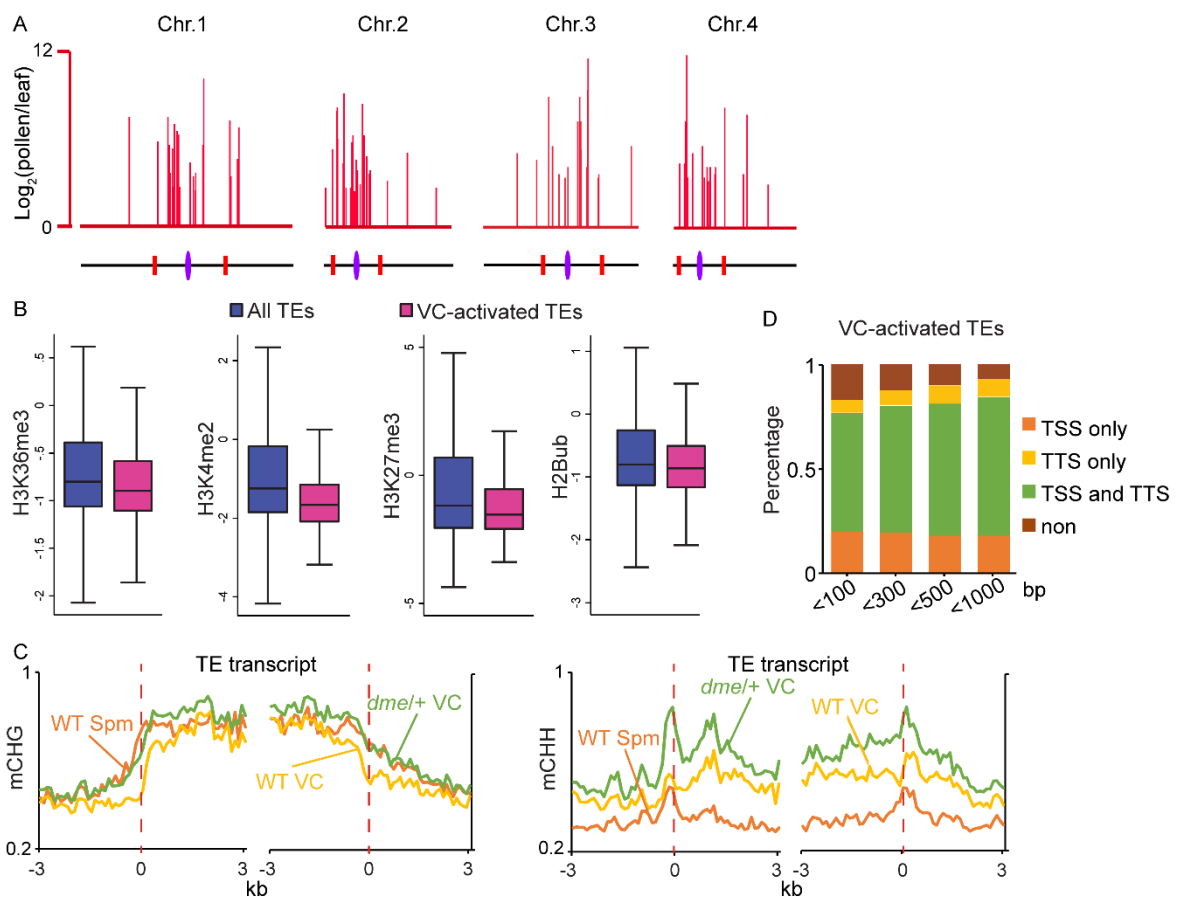
769 **Figure 1—source data 1.** List of VC-activated TEs.

770 **Figure 1—source data 2.** List of VC DME targets.

771 **Figure 1—figure supplement 1.** VC-activated TEs are heterochromatic and demethylated by  
 772 DME.

773

774 **Figure 1—figure supplement 1**

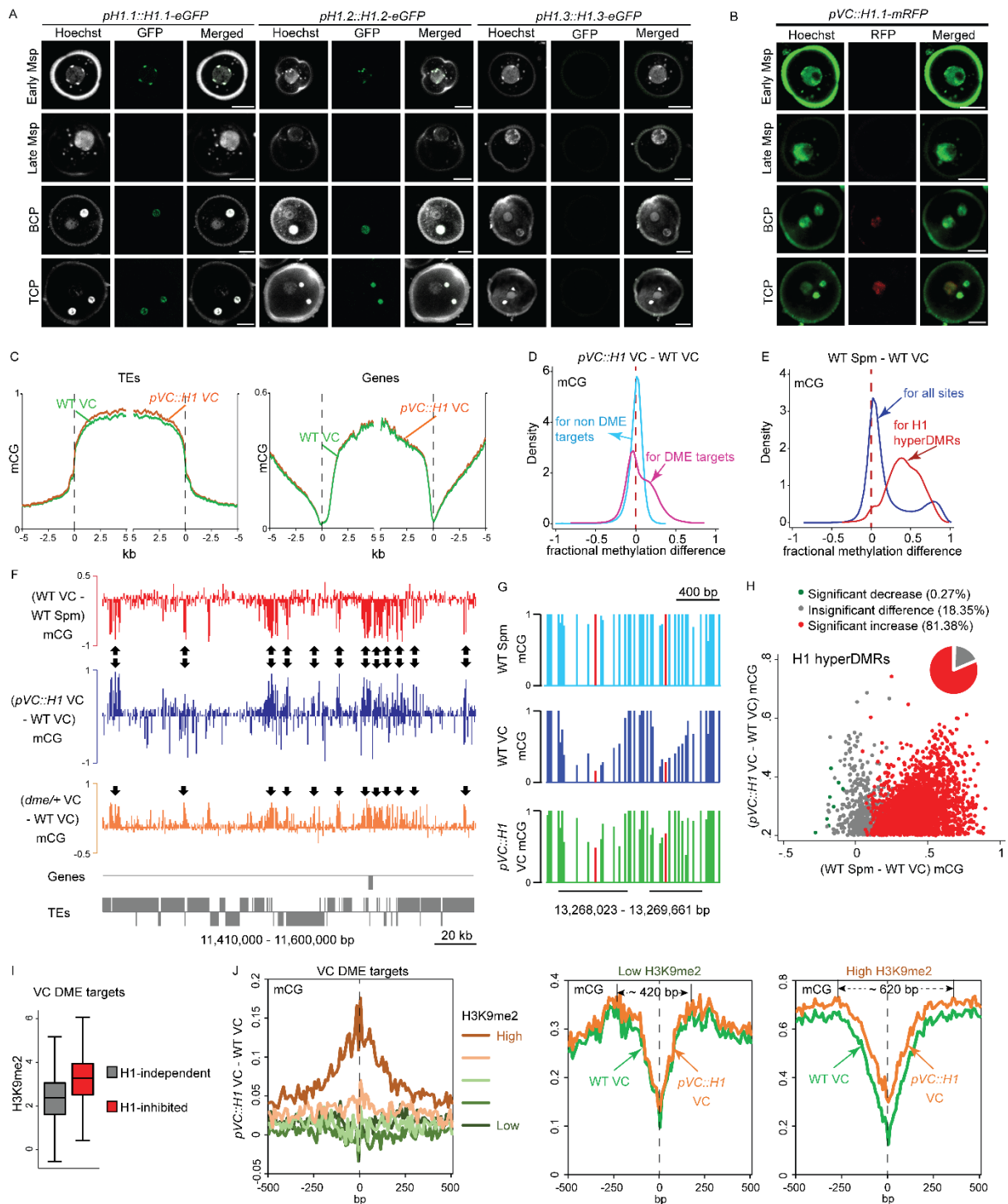


775

776 **Figure 1—figure supplement 1. VC-activated TEs are heterochromatic and demethylated by**  
 777 **DME.** (A) Chromosomal view of VC-activated TEs, similar to *Figure 1A*. (B) Box plots showing  
 778 the enrichment of euchromatic histone modifications at TEs, similar to *Figure 1B*. Difference  
 779 between the two datasets compared for each feature is significant (Kolmogorov-Smirnov test  $p <$   
 780 0.001). H2Bub, H2B ubiquitination. (C) Ends analysis of VC-activated TEs, similar to *Figure 1D*.  
 781 (D) Percentages of VC-activated TEs with TSS and/or TTS within indicated distances of VC DME  
 782 targets.

783

784 **Figure 2** with 2 supplements



785

786 **Figure 2. Ectopic H1 expression in the vegetative cell impedes DME at the most**  
 787 **heterochromatic loci. (A–B)** Confocal images showing H1 localization under native promoter (A)  
 788 and VC-specific promoter (*pVC*, B) during male gametogenesis. Msp, microspore; BCP, bicellular  
 789 pollen; TCP, tricellular pollen. Bars, 5  $\mu$ m. All *pVC::H1.1-mRFP* (short as *pVC::H1*) refers to line  
 790 #2. (C) Ends analysis of all TEs or genes in VCs from *pVC::H1* (line #2) and WT. (D–E) Kernel  
 791 density plots illustrating frequency distribution of methylation differences in 50bp windows  
 792 between VCs from *pVC::H1* and WT (D), and between WT sperm (Spm) and VC (E). (F)  
 793 Snapshots showing CG methylation difference between the indicated cell types. Arrows point to  
 794 DME targets that are hypermethylated by *pVC::H1*. (G) Snapshots demonstrating CG methylation



795 in sperm and VCs at single-nucleotide resolution, with the cytosine most hypomethylated by DME  
796 marked in red. VC DME targets are underlined in black. **(H)** Scatter plot illustrating CG  
797 methylation differences between the indicated cell types at H1 hyperDMRs. 82.25% of H1  
798 hyperDMRs show significant increase in sperm in comparison to VCs. **(I)** Box plot illustrating  
799 H3K9me2 level at VC DME targets that are significantly hypermethylated in *pVC::H1* (H1-  
800 inhibited) or not (H1-independent), respectively. Difference between the two groups is significant  
801 (Kolmogorov-Smirnov test  $p < 0.001$ ). **(J)** VC DME targets were grouped according to H3K9me2  
802 levels, aligned at the most demethylated cytosine (dashed lines), and plotted for average CG  
803 methylation difference as indicated in each 10-bp interval (left). Similarly, CG methylation in  
804 *pVC::H1* and WT VCs was plotted for the group with the lowest and highest H3K9me2,  
805 respectively. Spm, sperm.

806 The following figure source data and supplements are available for Figure 2:

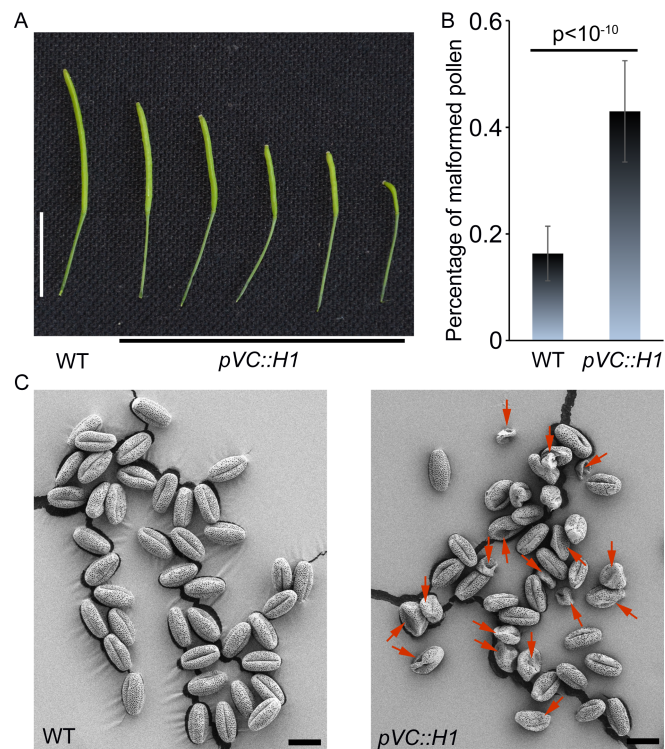
807 **Figure 2—source data 1.** List of H1 hyperDMRs.

808 **Figure 2—figure supplement 1.** H1 ectopic expression in the vegetative cell causes pollen defect  
809 and reduced fertility.

810 **Figure 2—figure supplement 2.** H1 ectopic expression in the vegetative cell causes DNA  
811 hypermethylation at DME targets.

812

813 **Figure 2—figure supplement 1**

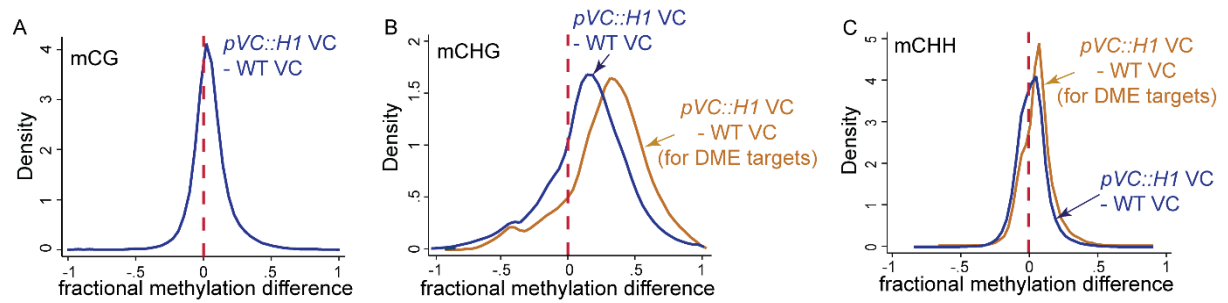


814

815 **Figure 2—figure supplement 1. H1 ectopic expression in the vegetative cell causes pollen**  
816 **defect and reduced fertility.** *pVC::H1* (*pLAT52::H1-mRFP* line #2) plants show reduced silique  
817 length (A) and an increased proportion of malformed pollen grains (B), which are indicated by red  
818 arrows in the SEM image (C). Student's *t* test  $p < 10^{-10}$ ;  $n = 17$ ; mean  $\pm$  SD are shown. Bar (A), 1 cm;  
819 Bar (C), 20  $\mu$ m.

820

821 **Figure 2—figure supplement 2**

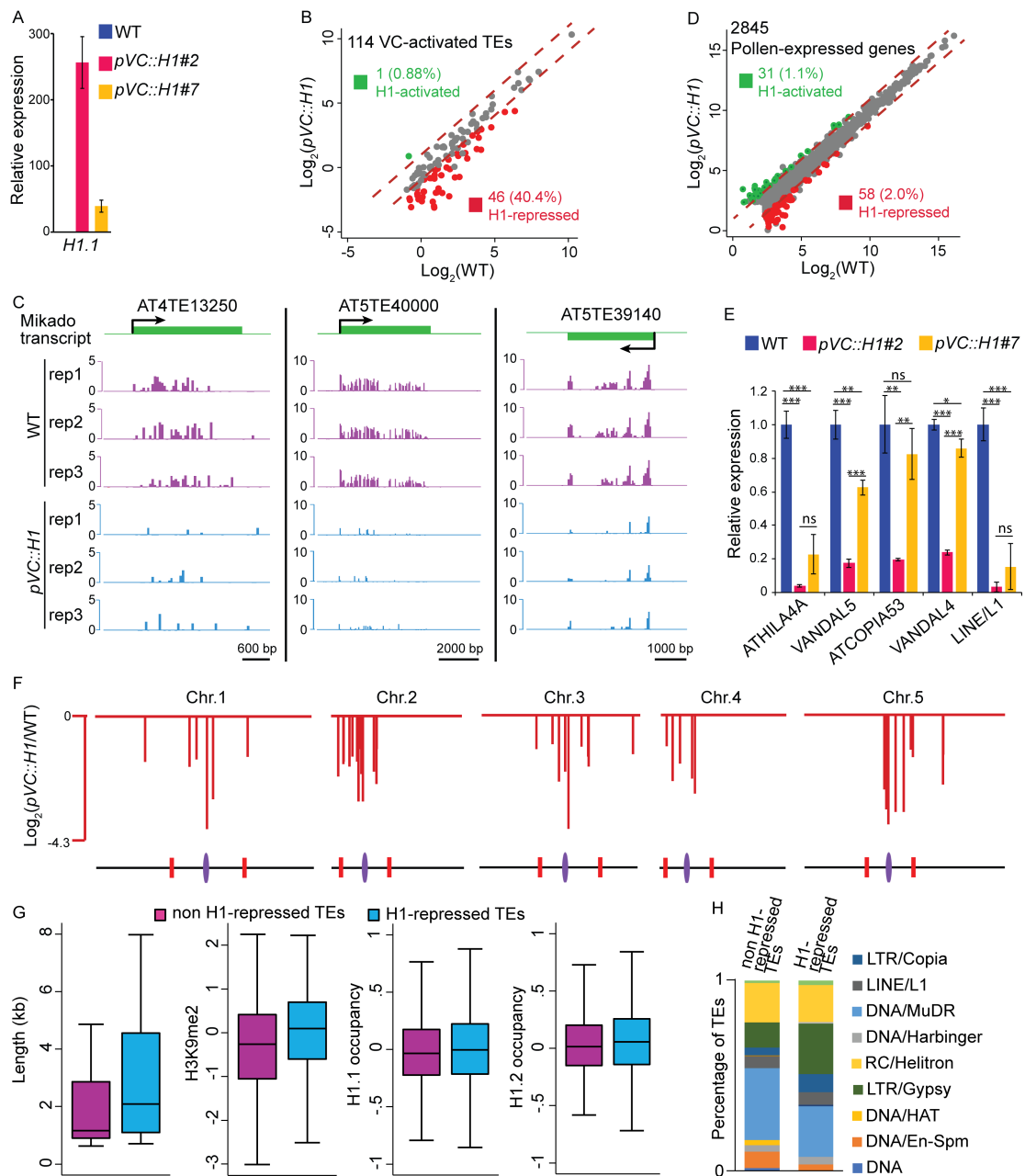


822

823 **Figure 2—figure supplement 2. H1 ectopic expression in the vegetative cell causes DNA**  
824 **hypermethylation at DME targets.** Kernel density plots showing frequency distribution of  
825 methylation differences between VCs from *pVC::H1* and WT in all 50-bp windows (blue traces)  
826 and windows overlapping VC DME targets (orange traces).

827

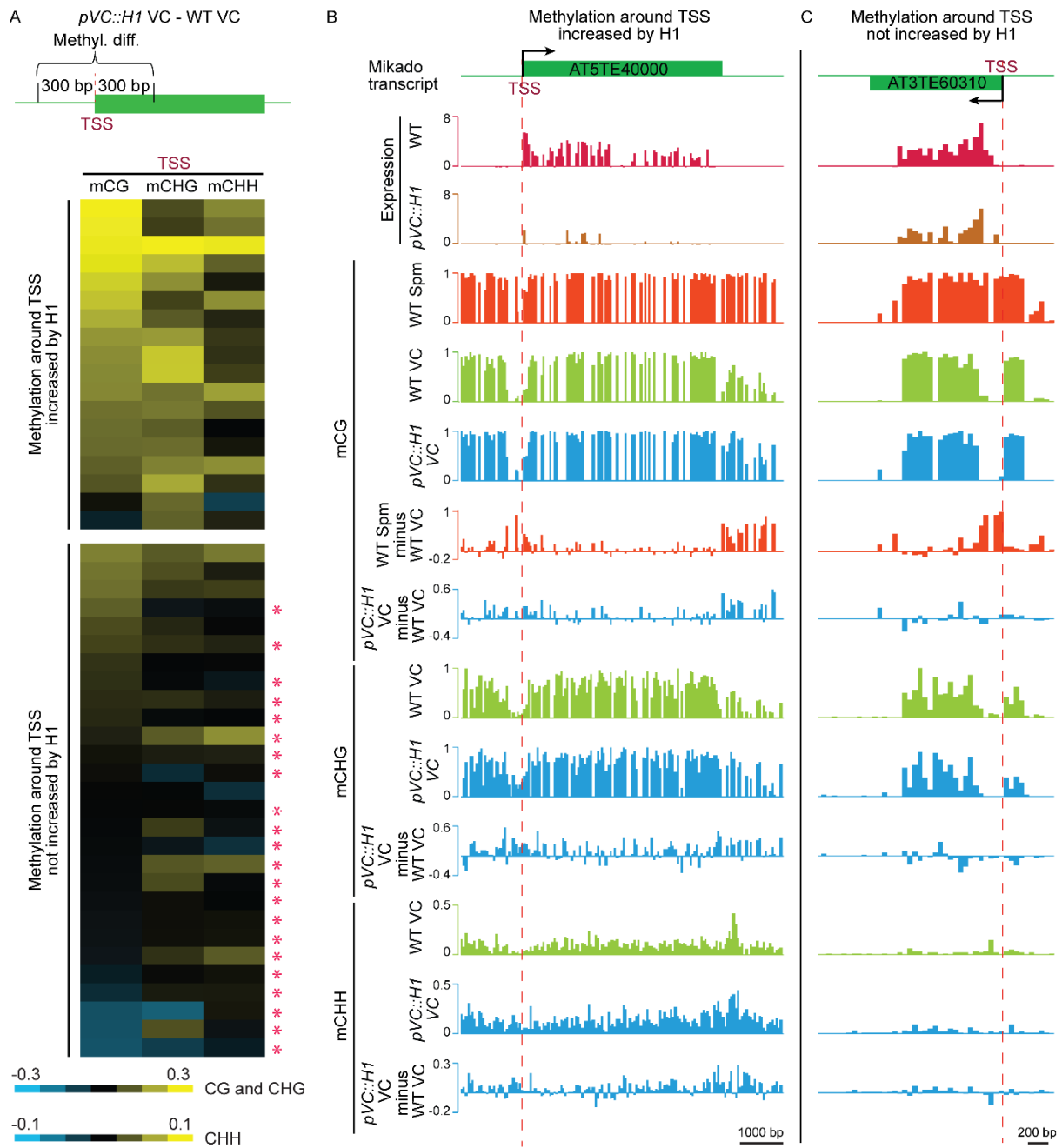
828 **Figure 3**



829

830 **Figure 3. Vegetative-cell-expressed H1 represses heterochromatic TEs in a dosage-dependent**  
 831 **manner.** *pVC::H1* refers to line #2 except as specified in **A** and **E**. (**A,E**) quantitative RT-PCR  
 832 demonstrating *H1.1* (**A**) or TE (**E**) expression in pollen from WT and two independent *pVC::H1*  
 833 transgenic lines. Relative expression is calculated by normalizing to WT (WT = 1). Student's *t* test  
 834 \**p*<0.05, \*\**p*<0.01, \*\*\**p*<0.001; ns, not significant; *n*=3; mean ± SD are shown. (**B,D**) Scatter plot  
 835 illustrating the expression ( $\text{Log}_2\text{TPM}$ ) of TEs or genes in WT and *pVC::H1* pollen. Red and green  
 836 dots indicate significant down- and up-regulation in *pVC::H1* compared to WT ( $|\text{fold change}| > 2$ ,  
 837 marked by dashed lines; likelihood ratio test *p* < 0.05), respectively. (**C**) Snapshots showing the  
 838 expression ( $\text{Log}_2\text{RPKM}$ ) of 3 example H1-repressed TEs in WT and *pVC::H1* pollen. Rep,  
 839 biological replicate. (**F**) Chromosomal view of H1-repressed TEs, similar to *Figure 1A*. (**G**) Box  
 840 plots illustrating the length, H3K9me2 enrichment, and H1 occupancy at two groups of VC-  
 841 activated TEs. Difference between the two datasets compared for each feature is significant  
 842 (Kolmogorov-Smirnov test *p* < 0.05 for length, and < 0.001 for others). (**H**) Percentages of TEs  
 843 classified by superfamily.

844 **Figure 4**

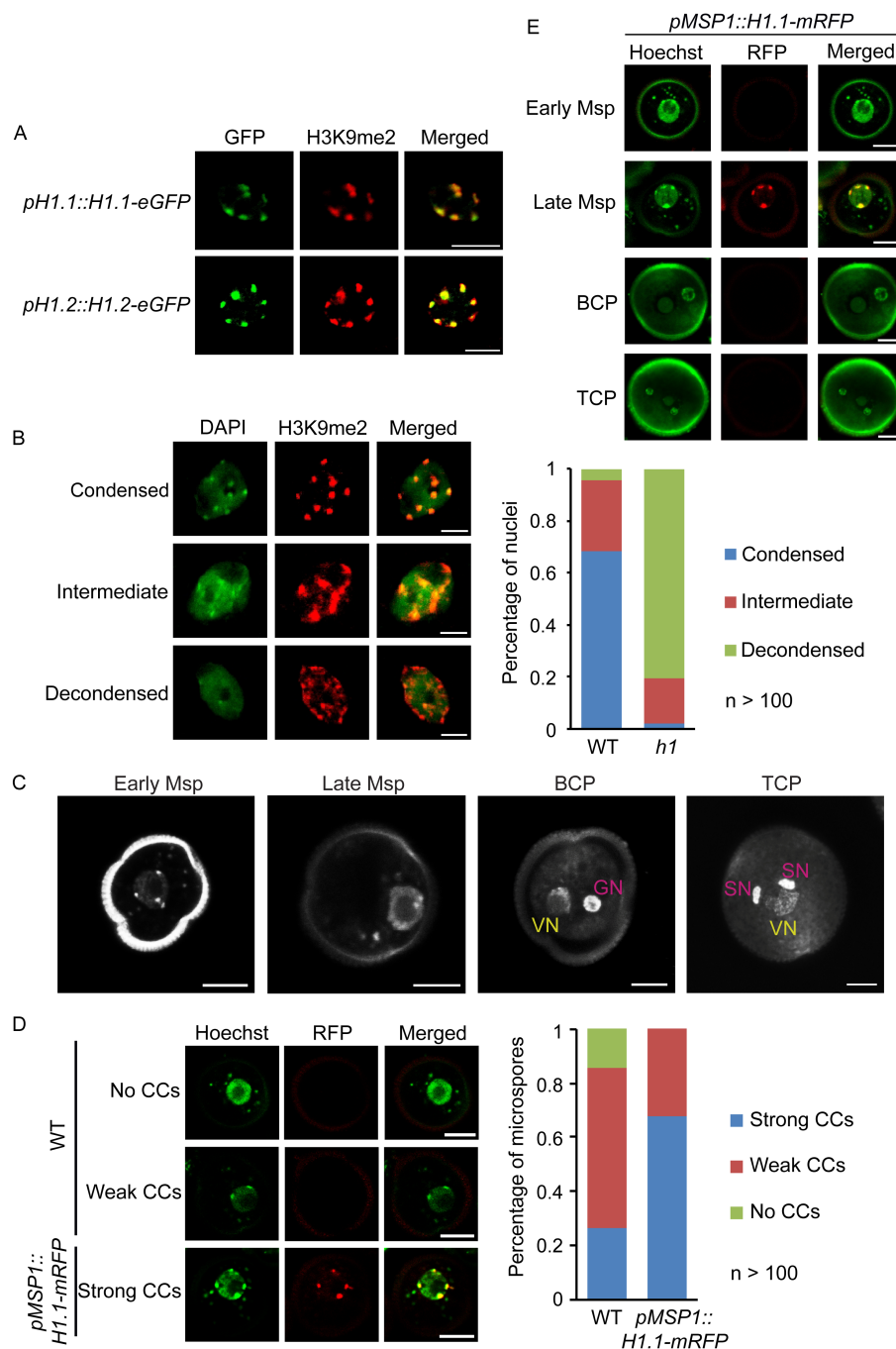


845

846 **Figure 4. H1 suppresses TEs in the vegetative cell via two mechanisms.** (A) Heat map  
 847 demonstrating DNA methylation differences between *pVC::H1* and WT VCs within 300 bp of the  
 848 TSS of H1-repressed TEs. Asterisks mark TEs whose suppression is not caused by changes in DNA  
 849 methylation. Data are sorted in descending order based on CG methylation difference for upper  
 850 and lower panels, respectively. (B,C) Snapshots showing the expression and DNA methylation of  
 851 representative TEs suppressed by *pVC::H1* via methylation-dependent (B) and -independent (C)  
 852 mechanisms, respectively. Spm, sperm.

853

854 **Figure 5**

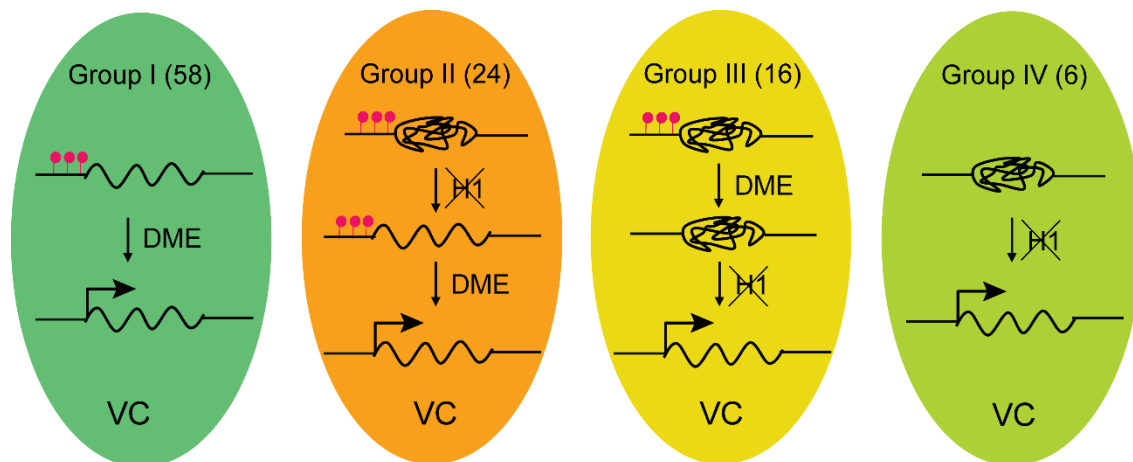


855

856 **Figure 5. Depletion of H1 decondenses heterochromatin in leaves and late microspores.** (A)  
 857 Immunostaining with GFP and H3K9me2 antibodies showing the co-localization of H1 and  
 858 H3K9me2-enriched chromocenters. (B) Examples of leaf nuclei with condensed, intermediate or  
 859 decondensed chromocenters, and their percentages in WT or the *h1* mutant. Msp, microspore; BCP,  
 860 bicellular pollen; TCP, tricellular pollen. (C) Gradual decondensation of heterochromatin during  
 861 male gametogenesis in *Arabidopsis*. Micrographs of Hoechst-stained microspores and pollen  
 862 demonstrate a gradual dispersion of chromocenters in late microspores and subsequently the  
 863 vegetative nucleus (VN) in pollen. Chromocenters are not detected in the VN of BCP and TCP.  
 864 GN, generative nucleus. (D) Percentages of late microspores with no, weak or strong  
 865 chromocenters (CCs; examples on the left) in WT and *pMSP1::H1.1-mRFP*, in which H1 co-  
 866 localizes with the strong CCs. (E) H1 is induced only in late microspores in *pMSP1::H1.1-mRFP*,  
 867 and co-localizes with strong CCs. All bars, 5  $\mu$ m.

868

869 **Figure 6**



870

871 **Figure 6. Model depicting four mechanisms underlying TE activation in the VC.** The number  
872 of TEs in each group is shown on the top. Significantly less heterochromatic than TEs in other  
873 groups (*Figure 3G*), Group I TEs are activated by DME-directed DNA demethylation. Group II  
874 TEs rely on H1 depletion to allow DME demethylation and activation. Group III TEs are  
875 demethylated by DME but require H1 depletion to allow transcription (ie. *pVC::H1* represses these  
876 TEs without affecting DME). Group IV TEs are not demethylated by DME; their activation is  
877 solely dependent on the depletion of H1. TEs belong to each group are listed in *Figure 1—source*  
878 *data 1*. Red lollipops denote DNA methylation.

879

880 **Supplementary file 1. Sequencing summary statistics for bisulfite sequencing libraries.**

881 Mean DNA methylation (Met) was calculated by averaging methylation of individual cytosines in  
882 each context, and chloroplast CHH methylation was used as a measure of cytosine non-conversion  
883 and other errors. SN, sperm nuclei; VN, vegetative nuclei.

Sample	Nuclear Genome Coverage	Nuclear CG Met	Nuclear CHG Met	Nuclear CHH Met	Chloroplast CHH Met
WT SN	37.0	24.7%	8.0%	1.1%	0.33%
WT VN	43.7	14.4%	5.2%	1.8%	0.45%
<i>pVC::H1</i> VN	62.6	16.1%	5.8%	1.9%	0.53%

884

885

886

887 **Supplementary file 2. List of primers for quantitative RT-PCR.**

Gene	Forward	Reverse
ATHILA4A	TTGGTGGGAAGAGGTTATCAG	GCTGAAACTACTGCTTTTCTG
VANDAL5	GATTACTGATGACCCCATG	CCTCATCATCTGGTTCATTG
ATCOPIA53	TCATATTATCTCTGATGGATC	ACCTGTTCCCTACCATGTG
VANDAL4	GCTTAGCTATCCACGCTATC	CGTCTTCATCTCATGGGAC
LINE/L1	CGATCATTCCTGGTCATTG	ACCCTTCTTTACTAATCCATC
TUA2	CCGTCTCGTCTCTCAGGTTATCTC	CGGAGATGACTGGGGCAT

888

889